

Astrophysical hydromagnetic turbulence

A. Brandenburg · A. Lazarian

September 10, 2018, Revision: 1.53

Abstract Recent progress in astrophysical hydromagnetic turbulence is being reviewed. The physical ideas behind the now widely accepted Goldreich–Sridhar model and its extension to compressible magnetohydrodynamic turbulence are introduced. Implications for cosmic ray diffusion and acceleration is being discussed. Dynamo-generated magnetic fields with and without helicity are contrasted against each other. Certain turbulent transport processes are being modified and often suppressed by anisotropy and inhomogeneities of the turbulence, while others are being produced by such properties, which can lead to new large-scale instabilities of the turbulent medium. Applications of various such processes to astrophysical systems are being considered.

Keywords magnetic fields · turbulence · Sun: magnetic fields · ISM: magnetic fields

PACS 44.25.+f · 47.27.Eq · 47.27.Gs · 47.27.Qb

1 Introduction

Hydromagnetic or magnetohydrodynamic (MHD) turbulence plays an important role in many astrophysical settings. In a recent review by Brandenburg and Nordlund (2011), properties of turbulence were discussed for the solar wind, stellar convection zones, the interstellar medium, accretion discs, galaxy clusters, and the early Universe. In an earlier review by Brandenburg and Subramanian (2005), a detailed account of dynamo theory with emphasis on helical dynamos was given. In that review, and also in Brandenburg et al. (2012c), the small-scale dynamo was discussed in detail. Applications to galactic dynamos were discussed by Beck et al. (1996). Aspects of magnetic reconnection and particle acceleration in turbulent flows have recently been reviewed by Lazarian et al. (2012b). In the present review we begin with turbulence in the interstellar medium, discuss how turbulence is affected by

A. Brandenburg

Nordita, KTH Royal Institute of Technology and Stockholm University, Roslagstullsbacken 23, 10691 Stockholm, Sweden; and Department of Astronomy, Stockholm University, SE 10691 Stockholm, Sweden, E-mail: brandenb@nordita.org

A. Lazarian

Department of Astronomy, University of Wisconsin-Madison
475 N. Charter St., Madison, WI 53706, USA E-mail: lazarian@astro.wisc.edu

magnetic fields and compressibility, address then applications to cosmic ray scattering and turn then to dynamo-generated magnetic fields as well as to anisotropic and inhomogeneous flows that are affected by stratification and rotation.

2 Turbulence in the interstellar medium

The ISM is turbulent on scales ranging from AUs to kpc (Armstrong et al. 1995; Elmegreen and Scalo 2004), with an embedded magnetic field that influences almost all of its properties. MHD turbulence is accepted to be of key importance for fundamental astrophysical processes, e.g. star formation, propagation and acceleration of cosmic rays. It is therefore not surprising that attempts to obtain spectra of interstellar turbulence have been numerous since the 1950s (Münch 1958). However, various directions of research achieved varying degrees of success. For instance, studies of turbulence statistics of ionized media accompanied by theoretical advancements in understanding scattering and scintillation of radio waves in ionized media (Goodman and Narayan 1985) were rather successful (cf. Spangler and Gwinn 1990). This work provided information about the statistics of the electron density on scales 10^8 – 10^{15} cm (Armstrong et al. 1995). These measurements have been recently combined with data from the Wisconsin H α Mapper, which also measures electron density fluctuation, but on larger scales. The resulting extended spectrum presented in Chepurnov and Lazarian (2010) shows that the Kolmogorov $-5/3$ spectrum of electron density fluctuations extends to several more decades to larger scales; see Figure 1.

In spite of their success, these sort of measurements provide only density statistics, which is a rather indirect measure of turbulence. Velocity statistics is a much more direct turbulence measure. Although it is clear that Doppler broadened lines are affected by turbulence, recovering the velocity statistics is extremely challenging without adequate theoretical insight. Indeed, both the z component of velocity and density contribute to fluctuations of the energy density $\rho_s(\mathbf{X}, V_z)$ in Position-Position-Velocity (PPV) space.

Traditionally, information on turbulence spectra is obtained using the measure of Doppler shifts termed Velocity Centroids, $\sim \int V_z \rho_s dV_z$, where the integration is taking place over the range of the velocities relevant to the object under study. In this situation it is easy to see that the Velocity Centroids are also proportional to $\int V_z \rho ds$, where ρ is the actual three-dimensional density and the integration is performed along the line of sight (Lazarian and Esquivel 2003).

Usually the Velocity Centroids are normalized by the intensity integrated over the line of sight (Stenholm 1990), and the work of Lazarian and Esquivel (2005) showed that this normalization does not change the statistical properties of the measure. However, the numerical and analytical analysis in Lazarian and Esquivel (2005) and Esquivel et al. (2007) showed that the Velocity Centroids fail for studying supersonic turbulence. This provides bad news for the studies of velocity statistics in molecular clouds and the diffuse cold ISM (Dickman and Kleiner 1985; Miesch et al. 1999; Miville-Deschênes et al. 2003). The studies for HII regions (O’dell and Castaneda 1987) are less strongly affected, as in most cases the turbulence there is subsonic.

There have been attempts to analyze PPV data cubes in other ways. For instance, Crovisier and Dickey (1983), Green et al. (1993), and Stanimirovic (1999) analyzed power spectra of velocity channels of HI data. The spatial spectrum of fluctuations of these velocity slices of PPV revealed power-law dependences, but the physical meaning of these dependences remained unclear. (Indeed, some of the authors erroneously identified the spectral index of intensity

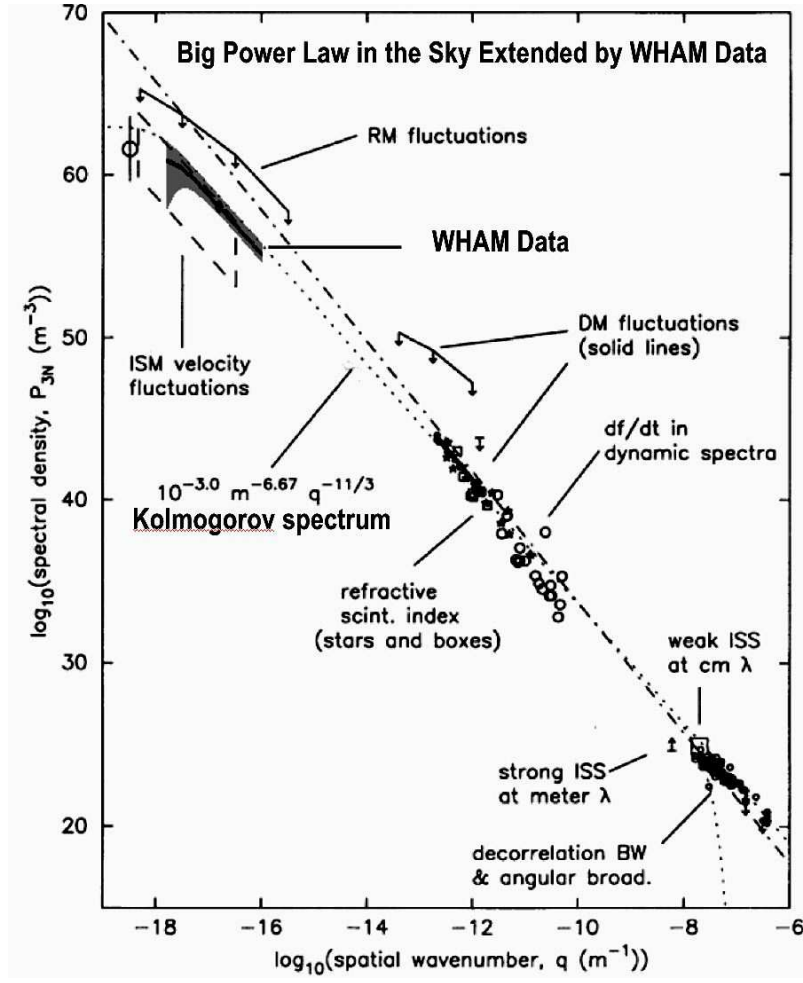


Fig. 1 Turbulence in the interstellar gas obtained from electron density fluctuations. The “Big Power Law in the Sky” of Armstrong et al. (1995) is here extended using data from the Wisconsin H α Mapper (WHAM). The slope corresponds to that of Kolmogorov turbulence. Adapted from Chepurnov and Lazarian (2010).

perturbations in slices of PPV data with the spectral index of the underlying turbulence spectrum. The nature of the variations of the spectral index in different studies was unclear.)

The analytical study of the statistical properties of the PPV energy density ρ_s has been initiated by Lazarian and Pogosyan (2000). There the observed statistics of ρ_s was related to the underlying 3D spectra of velocity and density in the astrophysical turbulent volume. Initially, the volume was considered transparent, but later the treatment was generalized to volumes with self-absorption and to studies of turbulence using absorption lines (Lazarian and Pogosyan 2004, 2006, 2008). The resulting theory of mapping of fluctuations in Position-Position-Position space with turbulent velocity into PPV space was successfully tested in a number of studies (Padoan et al. 2006, 2009; Chepurnov and Lazarian 2009; Burkhart et al. 2013). This theory lays the foundation for two separate techniques, Velocity Channel Analysis (VCA) and Velocity Correlation Spectrum (VCS) which were applied by

a number of groups to different data sets including HI, C O¹³, ¹⁸C O; see more in Lazarian (2009). The results can be briefly summarized as follows: the tested supersonic media exhibit a velocity spectrum that is steeper than the spectrum of Kolmogorov turbulence and a density spectrum that is shallower. This result is, in fact, expected for supersonic MHD turbulence (Beresnyak et al. 2005; Kowal et al. 2007).

We emphasize that VCA and VCS are two related techniques based on solid analytical foundations. The theory of the VCA in Lazarian and Pogosyan (2000, 2004) and VCS in Lazarian and Pogosyan (2006, 2008) describe the non-linear mapping provided by velocity fluctuations from the turbulent volume to the Position-Position-Velocity (PPV) space. Therefore the technique provides the true spectrum of velocity and density fluctuations, irrespectively of the sources and sinks of turbulence. The energy injection associated with localized injection of turbulence, e.g. with the outflows should be detected as the changes in the spectral slope corresponding to the scales of energy injection.

3 The picture of Alfvénic Turbulence

The picture of MHD turbulence has been developing over decades and pioneering works by Iroshnikov (1963) and Kraichnan (1965) are definitely to be mentioned. The Iroshnikov-Kraichnan model was the extension of Kolmogorov's *isotropic* turbulence model and it is the assumption of anisotropy that was a deficiency of this model. The notion of anisotropic turbulence was established later in important works, notably, by Shebalin et al. (1983) for incompressible turbulence and Higdon (1984) for the compressible turbulence. These papers provided the ground for the further advance.

Quantitative insight into MHD turbulence has been obtained in the seminal paper by Goldreich and Sridhar (1995), hereafter referred to as GS95. This paper quantified the properties of the anisotropic cascade and provided foundations for further theoretical development in the field. We may mention parenthetically that the original paper could not provide the perfect picture of MHD turbulence theory and a number of key aspects were clarified and corrected in subsequent studies. For instance, the original claim in GS95 and Goldreich and Sridhar (1997) about the role of 3-wave interactions were later corrected, and for weak MHD turbulence the point of view expressed in Ng and Bhattacharjee (1996) was adopted. Similarly, the notion of a *local* system of reference that is essential for understanding critical balance, which is a corner stone of our modern understanding of GS95 theory, was missing in the original paper. In fact, the closure relations that are used in GS95 to justify the model are written in the system of reference related to the mean field and therefore cannot be used as a proof. The importance of a local system of reference was understood only in subsequent theoretical and numerical studies by Lazarian and Vishniac (1999), henceforth LV99, Cho and Vishniac (2000), as well as Maron and Goldreich (2001).

3.1 Incompressible MHD turbulence

While having a long history of ideas, the theory of MHD turbulence has become testable recently with the advent of numerical simulations (Biskamp 2003), which confirmed (see Cho and Lazarian 2005, and references therein) the prediction of magnetized Alfvénic eddies being elongated in the direction of the magnetic field (Shebalin et al. 1983; Higdon 1984) and provided results consistent with quantitative relations for the degree of eddy elongation obtained by GS95.

MHD turbulence theory is in many respects similar to the famous Kolmogorov (1941) theory of turbulence. In the latter theory, energy is injected at large scales, creating large eddies which do not dissipate energy through viscosity¹ but transfer energy to smaller eddies. The process continues until the cascade reaches the eddies that are small enough to dissipate energy over an eddy turnover time. In the absence of compressibility the hydrodynamic cascade of energy is $\sim v_l^2/\tau_{\text{casc},l} = \text{const}$, where v_l is the velocity at the scale l and the cascading time for the eddies of size l is $\tau_{\text{casc},l} \approx l/v_l$. From this the well known relation $v_l \sim l^{1/3}$ follows.

In MHD turbulence, in the presence of dynamically important magnetic fields, eddies become anisotropic. At the same time, one can imagine eddies mixing magnetic field lines perpendicular to the direction of the magnetic field. For these eddies, the original Kolmogorov treatment is applicable resulting in perpendicular motions scaling as $v_l \sim l_\perp^{1/3}$, where l_\perp denotes eddy scales measured perpendicular to the magnetic field. These mixing motions induce Alfvénic perturbations that determine the parallel size of the magnetized eddy. A cornerstone of the GS95 theory is *critical balance*, i.e. the equality of the eddy turnover time l_\perp/v_l and the period of the corresponding Alfvén waves $\sim l_\parallel/V_A$, where l_\parallel is the parallel eddy scale and V_A is the Alfvén velocity. Making use of the earlier expression for v_l , one can easily obtain $l_\parallel \sim l_\perp^{2/3}$, which reflects the tendency of eddies to become more and more elongated as energy cascades to smaller scales.

It is important to stress that the scales l_\perp and l_\parallel are measured with respect to a system of reference related to the direction of the local magnetic field “seen” by the eddy. This notion was not present in the original formulation of the GS95 theory and was added to it later by Lazarian and Vishniac (1999), henceforth LV99, and Cho and Vishniac (2000). The local system of reference was also used in numerical studies in Cho and Vishniac (2000), Maron and Goldreich (2001), and Cho et al. (2002) that tested GS95 theory. In terms of mixing motions, it is rather obvious that the free Kolmogorov-type mixing is possible only with respect to the local magnetic field of the eddy rather than the mean magnetic field of the flow.

While the arguments above are far from being rigorous, they correctly reproduce the basic scalings of magnetized turbulence when the velocity is equal to V_A at the injection scale L . The most serious argument against this picture is the ability of eddies to perform mixing motions perpendicular to the magnetic field. This problem was addressed in LV99, where the self-consistency of the GS95 theory was related to fast reconnection of the magnetic field in turbulent fluids. A more rigorous discussion of a self-consistent treatment of MHD turbulence and magnetic reconnection is presented in Eyink et al. (2011).

The GS95 theory is formulated assuming isotropic injection of energy at scale L and the injection velocity equal to the Alfvén velocity in the fluid V_A , i.e. the Alfvén Mach number $M_A \equiv (V_L/V_A) = 1$, where V_L is the injection velocity. Thus, it provides the description of transAlfvénic turbulence. This model was later extended for both subAlfvénic, i.e. $M_A < 1$, and superAlfvénic, i.e. $M_A > 1$, cases (see LV99 and Lazarian 2006, respectively; see also Table 1). Indeed, if $M_A > 1$, then, instead of the driving scale L one can use the scale

$$l_A = LM_A^{-3}, \quad (1)$$

¹ The Reynolds number $\text{Re} \equiv L_f V/\nu = (V/L_f)/(\nu/L_f^2)$ characterizes the ratio of the eddy turnover rate $\tau_{\text{eddy}}^{-1} = V/L_f$ and the viscous dissipation rate $\tau_{\text{dis}}^{-1} = \eta/L_f^2$. Therefore large values of Re correspond to negligible viscous dissipation of large eddies over the cascading time τ_{casc} which is equal to τ_{eddy} in Kolmogorov turbulence.

Table 1 Regimes and ranges of MHD turbulence

Type of MHD turbulence	Injection velocity	Range of scales	Motion type	Ways of study
Weak	$V_L < V_A$	$[L, l_{\text{trans}}]$	wave-like	analytical
Strong subAlfvénic	$V_L < V_A$	$[l_{\text{trans}}, l_{\text{min}}]$	eddy-like	numerical
Strong superAlfvénic	$V_L > V_A$	$[l_A, l_{\text{min}}]$	eddy-like	numerical

L and l_{min} are injection and dissipation scales

l_{trans} and l_A are given by Equations (2) and (1), respectively.

which is the scale at which the turbulent velocity equals V_A . For $M_A \gg 1$, magnetic fields are not dynamically important at the largest scales and the turbulence at those scales follows the isotropic Kolmogorov cascade $v_l \sim l^{1/3}$ over the range of scales $[L, l_A]$. At the same time, if $M_A < 1$, the turbulence obeys GS95 scaling (also called “strong” MHD turbulence) not from the scale L , but from a smaller scale

$$l_{\text{trans}} = LM_A^2, \quad (2)$$

while in the range $[L, l_{\text{trans}}]$ the turbulence is “weak”.

The properties of weak and strong turbulence are rather different. Weak turbulence is wave-like turbulence with wave packets undergoing many collisions before transferring energy to small scales. Unlike strong turbulence, weak turbulence allows an exact analytical treatment (Galtier et al. 2000). By contrast, in strong turbulence intensive interactions between wave packets prevent the use of a perturbative approach. Numerical experiments have supported the GS95 ideas both for incompressible MHD turbulence (Cho and Vishniac 2000; Maron and Goldreich 2001; Cho et al. 2002; Beresnyak and Lazarian 2010; Beresnyak 2011) and for the Alfvénic component of compressible MHD turbulence (Cho and Lazarian 2002, 2003; Kowal and Lazarian 2010). [The compressible MHD turbulence simulations of Beresnyak et al. (2005) and Kowal et al. (2007) demonstrated that the density spectrum becomes more shallow and isotropic as the Mach number increases.]

While there are ongoing debates whether the original GS95 theory must be modified to better describe MHD turbulence, we believe that we do not have compelling evidence that GS95 is not adequate. The most popular one is the modification of the GS95 model by Boldyrev (2005, 2006), who, motivated by the spectral index of $-3/2$ observed in simulations of Maron and Goldreich (2001), proposed that the difference of the GS95 predictions and the numerical experiments arises from the dynamical alignment of velocity and magnetic fields. However, Beresnyak and Lazarian (2009, 2010) showed that present day numerical simulations may not have enough resolution to reveal the actual inertial range of MHD turbulence and the existing numerical simulations may be dominated by the bottleneck effect that distorts the actual slope of turbulence. Incidentally, the bottleneck effect already played a trick with the researchers when supersonic simulations suggested a $-5/3$ spectrum of supersonic turbulence (Boldyrev et al. 2002) which later was proven to be a bottleneck effect of shock wave turbulence with the expected -2 spectrum (Kritsuk et al. 2007). Such a spectrum has been confirmed with several different codes (Kritsuk et al. 2011). In addition, the $-5/3$ spectral index agrees well with the resolution studies by Beresnyak (2011, 2012). Thus, within the present review we will refer to GS95 when we shall talk about strong MHD turbulence.

The issue of the spectral slope is of both theoretical and practical importance. Although the differences between spectral slopes of $5/3$ and $3/2$ or even 2 do not look large, they correspond to very different physical pictures. The spectrum of $3/2$ corresponds to interactions

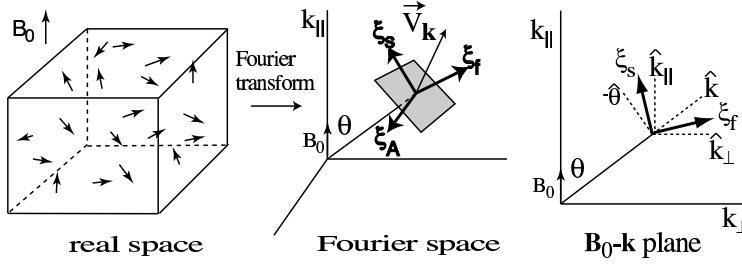


Fig. 2 Graphical representation of the mode separation method. We separate the Alfvén, slow and fast modes by the projection of the velocity Fourier component \mathbf{v}_k on the bases $\hat{\xi}_A$, $\hat{\xi}_s$ and $\hat{\xi}_f$, respectively. Adapted from CL03.

decreasing with the scale of turbulent motions, 5/3 corresponds to a strongly Kolmogorov-type picture of eddies, while 2 corresponds to a spectrum of shocks. The anisotropies predicted in these different pictures of turbulence are also different. They are in fact extremely important for cosmic ray propagation; see Yan and Lazarian (2004) and references therein. We also note that even a small difference in the slope can result in substantial differences in the energy at small scales due to the enormous extent of the astrophysical turbulent cascade. Finally, as GS95 has now the status of the accepted model of turbulence, it is essential to test all the predictions of this theory, including the predicted 5/3 spectral slope.

Usually, one considers balanced turbulence, i.e. the situation when the flows of energy in opposite directions are equal. In a more general case the turbulence is imbalanced, i.e. the flow of energy from one side dominates the flow from the opposite direction. The existing models of imbalanced turbulence are hotly debated at the moment and their predictions are being tested (Lithwick et al. 2007; Beresnyak and Lazarian 2008; Perez and Boldyrev 2009). Here we will just mention that in the case of astrophysical turbulence, compressibility may decrease the degree of imbalance, making the simple GS95 model applicable in spite of the presence of sources and sinks of energy.

3.2 Compressible MHD turbulence

The statistical decomposition of 3D MHD turbulence into fundamental modes, i.e. Alfvén, slow and fast, was performed in Fourier space by Cho and Lazarian (2002, 2003), henceforth CL02 and CL03, respectively, and later using wavelets by Kowal and Lazarian (2010). The idea of the decomposition is presented in Figure 2. The procedure was tested with the decomposition in real space in special cases when such a decomposition was possible, for instance, in the case of slow modes in a low plasma- β medium.

The most important result of this decomposition was establishing the relevance of Alfvénic turbulence scaling to a compressible medium. As we see in Figure 3, the anisotropy of the Alfvénic component corresponds to the GS95 predictions. In general, the study of transAlfvénic turbulence with different Mach numbers in CL02 and CL03 revealed that GS95 scaling is valid for *Alfvén modes*:

$$\text{Alfvén: } E^A(k) \propto k^{-5/3}, \quad k_{\parallel} \propto k_{\perp}^{2/3}.$$

Slow modes also follow the GS95 model for both high β and mildly supersonic low β cases:

$$\text{Slow: } E^S(k) \propto k^{-5/3}, \quad k_{\parallel} \propto k_{\perp}^{2/3}.$$

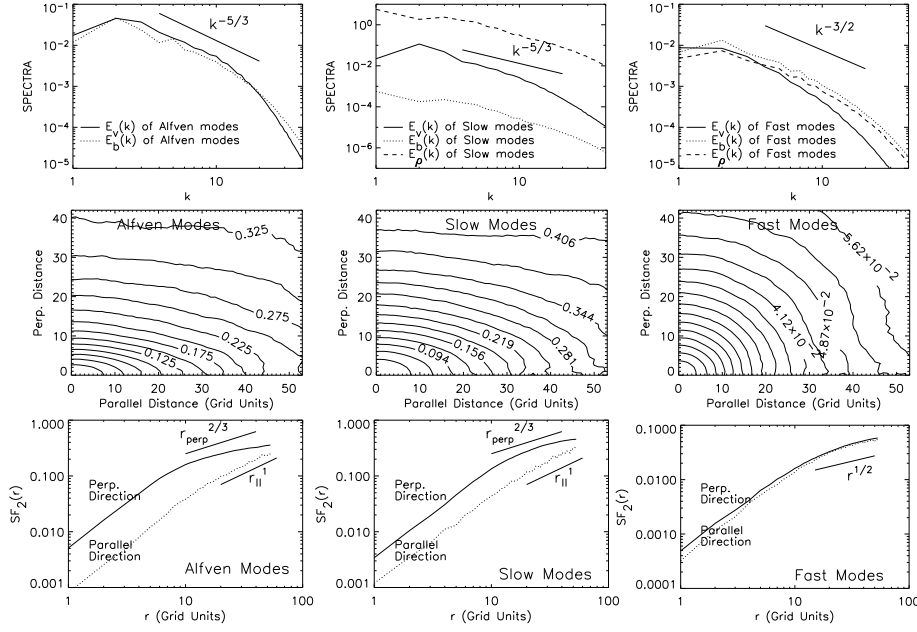


Fig. 3 Highly supersonic low β ($\beta \sim 0.02$ and $M_s \sim 7$). $V_A \equiv B_0/\sqrt{4\pi\rho} = 1$. a (sound speed) = 0.1. $\delta V \sim 0.7$. Alfvén modes follow the GS95 scalings. Slow modes follow the GS95 anisotropy. Fast modes are isotropic.

For the highly supersonic low β case, the kinetic energy spectrum of slow modes tends to be steeper, which may be related to the formation of shocks.

Fast mode spectra are compatible with acoustic turbulence scaling relations:

$$\text{Fast: } E^f(k) \propto k^{-3/2}, \text{ isotropic spectrum.}$$

The coupling between fast and Alfvén modes was shown to be weak and therefore the cascades of fast and Alfvén modes weakly affect each other (CL02). At the same time, Alfvén modes cascade to slow modes, which are otherwise passive in the cascade. This corresponds to the theoretical expectations discussed in GS95, Lithwick and Goldreich (2003), and CL03.

In terms of energy transfer from Alfvénic to compressible modes CL02 suggested the theory-motivated expression

$$\frac{\delta E_{\text{comp}}}{\delta E_{\text{Alf}}} \approx \frac{\delta V_A V_A}{V_A^2 + c_s^2}, \quad (3)$$

where δE_{comp} and δE_{Alf} are the energies of compressible and Alfvén modes, respectively. Equation (3) suggests that the drain of energy from Alfvénic cascade is marginal when the amplitudes of perturbations are weak, i.e. $(\delta V)_A \ll V_A$. Results of numerical calculations in CL02 are consistent with the expression above. The marginal transfer of energy between Alfvénic and compressible motions justifies considering the Alfvénic and fast cascades separately.

Higher resolution simulations in Kowal and Lazarian (2010) used a different wavelet-based decomposition technique. The results agree well with those in CL03. The advantage of the wavelet decomposition is the ability to decrease the error for the case of strongly perturbed fields.

4 Implications of MHD turbulence for diffusion processes

4.1 Diffusion of heat by MHD turbulence

Transport processes are known to be affected by turbulence. A big issue related to MHD turbulence is the nature of turbulent eddies. If magnetic field lines are perfectly frozen into fluid, then one cannot talk about mixing motions at the scale of dynamically important magnetic fields. On the contrary, if magnetic reconnection is fast enough to resolve the knots of intersecting magnetic fluxes that naturally arise in GS95 turbulence, mixing motions perpendicular to the local magnetic field should be similar to those in hydrodynamical fluids. This problem was addressed in LV99, where it was shown that magnetic reconnection induced by turbulence makes the GS95 picture of a perpendicular cascade self-consistent. A more recent study by Eyink et al. (2011) revealed the deep connection between turbulence and magnetic reconnection. This provides a theoretical justification for discussing hydrodynamic-type turbulent advection of heat in the presence of dynamically important magnetic fields.²

In addition, in hot plasmas, the motion of electrons along wandering magnetic fields is important. The statistics of magnetic field wandering was described in LV99 for different regimes of turbulence and provides the necessary foundations for a quantitative description of the heat transfer process. This is the process that we start our discussion with.

Let us initially disregard the dynamics of fluid motions on diffusion, i.e. we consider diffusion induced by particles moving along wandering turbulent magnetic field lines, whose motions we disregard for the sake of simplicity. Magnetized turbulence with a dynamically important magnetic field is anisotropic with eddies elongated along the direction of local magnetic field (henceforth denoted by \parallel), i.e. $l_{\perp} < l_{\parallel}$, where \perp denotes the direction perpendicular to the local magnetic field. Consider isotropic injection of energy at the outer scale L and dissipation at the scale $l_{\perp,\min}$. This scale corresponds to the minimal dimension of the turbulent eddies.

Initially, the problem of heat transport by electrons moving in turbulent magnetic fields was considered by Narayan and Medvedev (2001) for transAlfvénic turbulence. The treatment for both subAlfvénic and superAlfvénic turbulence was presented in Lazarian (2006); henceforth L06.

It is easy to notice that the separations of magnetic field lines at scales below the damping scale of turbulence, i.e. for $r_0 < l_{\perp,\min}$, are mostly influenced by the motions at the smallest scale. This scale $l_{\perp,\min}$ results in Lyapunov-type growth $\sim r_0 \exp(l/l_{\parallel,\min})$. This growth is similar to that obtained in earlier models with a single scale of turbulent motions; see Rechester and Rosenbluth (1978), henceforth RR78, and Chandran and Cowley (1998). Indeed, as the largest shear that causes field line divergence is due to the marginally damped motions at the scale around $l_{\perp,\min}$ the effect of larger eddies can be neglected and we are dealing with the case of single-scale “turbulence” described by RR78.

The electron Larmor radius presents the minimal perpendicular scale of localization, while the other relevant scale is the Ohmic diffusion scale corresponding to the scale of damped motions. Thus, conservatively it is natural to associate r_0 with the size of the cloud of electrons of the electron Larmor radius $r_{\text{Lar,particle}}$. Applying the original RR78 theory,

² The arguments in Eyink et al. (2011) should be distinguished from the arguments based on attempted renormalization of the effective magnetic Reynolds numbers in Blackman and Field (2008). Eyink et al. (2011) do not introduce artificial “turbulent diffusivities” but appeal to the established and tested concept of Richardson diffusion.

they found that the electrons should travel over a distance

$$L_{\text{RR}} \sim l_{\parallel, \text{min}} \ln(l_{\perp, \text{min}}/r_{\text{Lar}, e}) \quad (4)$$

to get separated by $l_{\perp, \text{min}}$.

Within the single-scale “turbulence model”, which formally corresponds to $L_{\text{ss}} = l_{\parallel, \text{min}} = l_{\perp, \text{min}}$, the distance L_{RR} is called Rechester–Rosenbluth distance. For the intracluster medium parameters, for which the problem was discussed originally, the logarithmic factor in Equation (4) is of the order of 30. This causes a 30-fold decrease of the thermal conductivity for the single-scale models³.

The single-scale turbulence model is just a toy model to study the effects of turbulent motions. However, one can use this model to describe what is happening below the scale of the smallest eddies. Indeed, shear and, correspondingly, magnetic field line divergence are maximal for the marginally damped eddies at the dissipation scale. Thus, for scales less than the damping scale the action of the critically damped eddies is dominant and the results of Equation (4) are applicable. The additional traveling distance of L_{RR} is of marginal importance for diffusion of heat over distances $\gg L_{\text{RR}}$.

For the diffusion in superAlfvénic turbulence the Alfvénic scale l_A given by Equation (1) is important. It acts as the characteristic scale of magnetic fluctuations. Assuming that the mean free path of electrons is less than l_A , L06 obtained:

$$\kappa_e \equiv \Delta^2/\delta t \approx (1/3)l_A v_e, \quad l_A < \lambda, \quad (5)$$

where v_e is the electron velocity. In the opposite limit of effective scattering $\lambda < l_A$, we have $\kappa \sim \lambda v_e$ with the coefficient of proportionality equal to $1/5$ according to Narayan and Medvedev (2001).

For subAlfvénic turbulence, the turbulence gets into the regime of strong GS95 type turbulence, which is described by Equation (2). The diffusivity becomes anisotropic with the diffusion coefficient parallel to the mean field, $\kappa_{\parallel, \text{particle}} \approx 1/3\kappa_{\text{unmagn}}$ being larger than the coefficient for diffusion perpendicular to the magnetic field (L06):

$$\kappa_{\perp, e} = \kappa_{\parallel, e} M_A^4, \quad M_A < 1, \quad (6)$$

As discussed above, turbulent motions themselves can induce advective transport of heat. Appealing to the LV99 model of reconnection, one can conclude that turbulence with $M_A \sim 1$ should be similar to hydrodynamic turbulence, i.e.

$$\kappa_{\text{dynamic}} \approx C_{\text{dyn}} LV_L, \quad M_A > 1, \quad (7)$$

where $C_{\text{dyn}} \sim 0(1)$ is a constant, which for hydro turbulence is around $1/3$ (Lesieur 1990). If we deal with heat transport, for fully ionized non-degenerate plasmas we assume $C_{\text{dyn}} \approx 2/3$ to account for the advective heat transport by both protons and electrons.

The advection of heat in the regime of subAlfvénic turbulence is reduced compared to the superAlfvénic case and given by expression (L06):

$$\kappa_{\text{dynamic}} \approx (\beta/3) LV_L M_A^3, \quad M_A < 1, \quad (8)$$

where $\beta \approx 4$.

Figure 5 illustrates the existing ideas on processes of heat conduction in astrophysical plasmas. They range from heat insulation by unrealistically laminar magnetic field (a), to

³ For the single-scale model, $L_{\text{RR}} \sim 30L$ and the diffusion over distance Δ takes $L_{\text{RR}}/L_{\text{ss}}$ steps, i.e. $\Delta^2 \sim L_{\text{RR}}L$, which decreases the corresponding diffusion coefficient $\kappa_{e, \text{single}} \sim \Delta^2/\delta t$ by a factor 30.

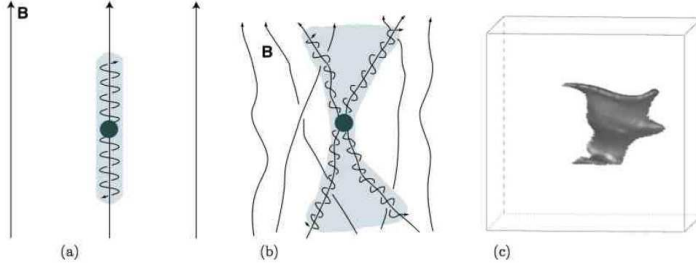


Fig. 4 Enßlin and Vogt (2006). (a) Textbook picture of electrons moving along magnetic field lines in thermal conduction process. (b) Actual motions of electrons in realistic turbulent plasmas where reconnection and spontaneous stochasticity of magnetic field are present. (c) Numerical simulations of heat advection in magnetized turbulence. From Cho and Lazarian (2004).

heat diffusion in turbulent magnetic field (b) and to heat advection by turbulent flows (c). field, to heat diffusion in turbulent magnetic field and to heat advection by turbulent flows. The relative efficiencies of the two latter processes depend on parameters of the turbulent plasma. The observational data for two clusters are also shown and it is clear that for the clusters of galaxies discussed, the turbulent advection of heat is the dominant process. The dominance of turbulent motions gets even more prominent if one takes into account that instabilities in the collisionless plasma of galaxies are likely to dramatically decrease the mean free path of electrons.

In thermal plasma, electrons are mostly responsible for thermal conductivity. The schematics of the parameter space for $\kappa_{\text{particle}} < \kappa_{\text{dynamic}}$ is shown in Figure 5, where the Mach number M_s and the Alfvén Mach number M_A are the variables. For $M_A < 1$, the ratio of diffusivities arising from fluid and particle motions is $\kappa_{\text{dynamic}}/\kappa_{\text{particle}} \sim \beta\alpha M_s M_A (L/\lambda)$; see Equations (6) and (8). The square root of the ratio of the electron to proton mass $\alpha = (m_e/m_p)^{1/2}$, which provides the separation line between the two regions in Fig. 2, is given by $\beta\alpha M_s \sim (\lambda/L)M_A$. For $1 < M_A < (L/\lambda)^{1/3}$ the mean free path is less than l_A which results in κ_{particle} being some fraction of κ_{unmagn} , while κ_{dynamic} is given by Equation (7). Thus $\kappa_{\text{dynamic}}/\kappa_{\text{particle}} \sim \beta\alpha M_s (L/\lambda)$, i.e. the ratio does not depend on M_A (horizontal line in Figure 5). When $M_A > (L/\lambda)^{1/3}$ the mean free path of electrons is constrained by l_A . In this case $\kappa_{\text{dynamic}}/\kappa_{\text{particle}} \sim \beta\alpha M_s M_A^3$; see Equations (7) and (5). This results in the separation line $\beta\alpha M_s \sim M_A^{-3}$ in Figure 5.

The application of the MHD approach to turbulent plasma has of course its limitations. For instance, in terms of magnetic reconnection, it is shown in Eyink et al. (2011) that the model of turbulent reconnection described in LV99 is applicable to current sheets if the broadening of the current sheet introduced through the wandering of magnetic field lines is larger than the Larmor radius of thermal ions. This makes the model not applicable to magnetosphere, where more sophisticated, e.g. based on PIC simulations, modeling is required.

4.2 Diffusion of magnetic fields in turbulent molecular clouds

MHD turbulence induces not only mixing motions advecting heat, but it also induces the transport of magnetic field and matter in molecular clouds. This process, first discussed in Lazarian (2005) and Lazarian and Vishniac (2009), was later tested numerically in Santos-Lima et al.

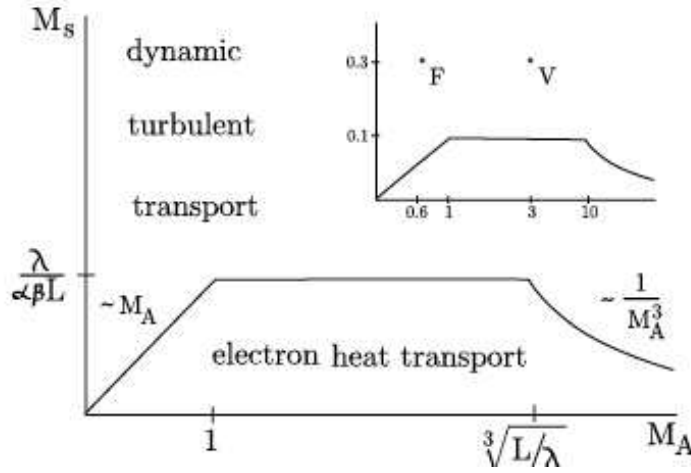


Fig. 5 Parameter space for particle diffusion or turbulent diffusion to dominate: application to heat transfer. Sonic Mach number M_s is plotted against the Alfvén Mach number M_A . The heat transport is dominated by the dynamics of turbulent eddies is above the curve (area denoted “dynamic turbulent transport”) and by thermal conductivity of electrons is below the curve (area denoted “electron heat transport”). Here λ is the mean free path of the electron, L is the driving scale, and $\alpha = (m_e/m_p)^{1/2}$, $\beta \approx 4$. *Example of theory application:* The panel in the right upper corner of the figure illustrates heat transport for the parameters for a cool core Hydra cluster (point “F”), “V” corresponds to the illustrative model of a cluster core in Enßlin and Vogt (2006). Relevant parameters were used for L and λ . From L06.

(2010, 2012) and showed high efficiency for removing magnetic fields from clouds and accretion disks. Lazarian et al. (2012a) showed that the process that they termed “reconnection diffusion” can explain why in observations by Crutcher et al. (2010) the envelopes had a lower mass to flux ratio than the cloud cores. In contrast, the usually considered ambipolar diffusion process predicts the opposite situation.

The elementary process of reconnection diffusion is illustrated in Figure 6, where the densities of plasma along magnetic flux tubes belonging to different eddies are different. The process of fast turbulent reconnection (LV99) creates new flux tubes with columns of entrained dense and rarefied plasmas. The situation is similar to the earlier discussed case with plasma moving along magnetic fields and equalizing the pressure within the newly formed flux tubes. As a result, eddies with initially different plasma pressures exchange matter and equalize the plasma pressure. This process can be described as the diffusion of plasma perpendicular to the mean magnetic field. In reality, for turbulence with the extended inertial range, the shredding of the columns of plasmas with different density proceeds at all turbulence scales, making the speed of plasma motion irrelevant for the diffusion. For the case of strong turbulence, the diffusion of matter and magnetic field is given by Equation (8). In the presence of the gravitational potential, the matter gets concentrated towards the center of the potential well. This was seen in the numerical simulations in Santos-Lima et al. (2010). The physical justification of the process is based on the nature of the GS95 cascade and the LV99 model of turbulent reconnection. The deep relation between the two is discussed in Eyink et al. (2011).

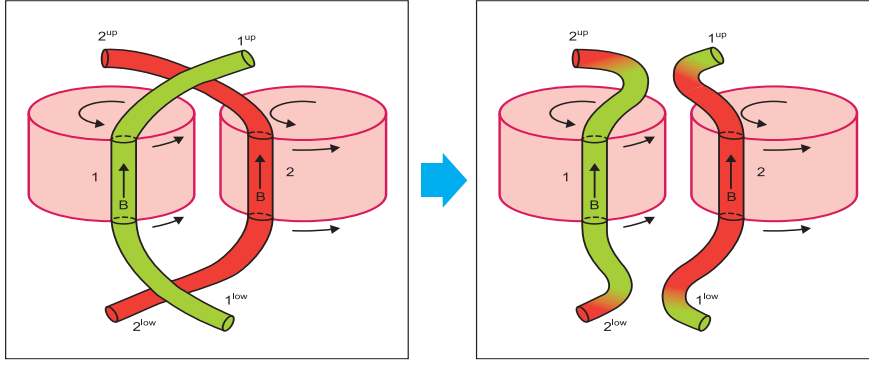


Fig. 6 Reconnection diffusion: exchange of flux with entrained matter. Illustration of the mixing of matter and magnetic fields due to reconnection as two flux tubes of different eddies interact. Only one scale of turbulent motions is shown. In real turbulent cascade such interactions proceed at every scale of turbulent motions. From Lazarian et al. (2012b).

4.3 Cosmic ray scattering, acceleration and perpendicular diffusion

MHD turbulence plays an important role in accelerating energetic particles. First of all, the second order Fermi acceleration can arise directly from the scattering of particles by turbulence (Melrose 1968). Properties of MHD turbulence that we discussed above are essential to understanding this process. If turbulence is injected at large scales, the anisotropy of Alfvénic modes at small scales makes them inefficient for scattering and acceleration of cosmic rays (Chandran 2000; Yan and Lazarian 2002)⁴. In this situation, fast modes were identified in Yan and Lazarian (2002) as the major scattering and acceleration agent for cosmic rays and energetic particles in interstellar medium (see also Yan and Lazarian 2004, 2008). This conclusion was extended for solar environments in Petrosian et al. (2006) and intracluster medium in Brunetti and Lazarian (2007). Turbulent magnetic field in the pre-shock and post-shock environment are important for the first order Fermi acceleration associated with shocks (Schlickeiser 2002). In particular, magnetic field enhancement compared to its typical interstellar values is important in the pre-shock region for the acceleration of high energy particles. The turbulent dynamo can provide a way of generating magnetic field in the precursor of the shock. In Beresnyak et al. (2009) it was shown that the interactions of the density inhomogeneities pre-existing in the interstellar medium with the precursor generate strong magnetic fields in the shock precursor, which allows particle acceleration up to the energy of 10^{16} eV.

While discussing heat transport by thermal electrons streaming along turbulent magnetic fields, we have discussed the perpendicular diffusion that is also relevant for the turbulent transport of cosmic rays perpendicular to the mean magnetic field. The relation between the parallel and perpendicular diffusivities in this case is also given by Equation (6); see Yan and Lazarian (2008). The important factor in this equation is M_A^4 . This dependence follows from the modern theory of MHD turbulence and it is very different from the dependence of M_A^2 discussed in the literature (Jokipii 1974).

⁴ The resonant scattering is happening on the magnetic scales of the order of the cosmic ray gyroradius. If the Alfvénic eddies are strongly elongated, the particles interact with many eddies within its radius and the scattering effect is dramatically reduced. Scattering efficiency and the acceleration efficiencies are closely related for the second order Fermi acceleration of cosmic rays by turbulence (see Schlickeiser 2006).

A stream of cosmic ray protons propagating parallel or antiparallel to a large-scale magnetic field can lead to important instabilities such as the Bell instability (Bell 2004). This is reviewed extensively in a companion paper by Bykov et al. (2013). The combined presence of a cosmic ray current and a parallel magnetic field gives rise to a pseudoscalar in the problem, and hence to an α effect which can lead to large-scale dynamo action (Rogachevskii et al. 2012). In the following, we discuss magnetic field amplification by dynamo action in more detail.

5 MHD turbulence with dynamo-generated magnetic fields

In this section we discuss the case where the magnetic field is produced self-consistently by the action of turbulence through dynamo action. We discuss here mainly the results of numerical simulations.

5.1 Definitions and conventions

In the following we characterize turbulent flows by the Reynolds number, which quantifies the ratio of advective to viscous accelerations, $\mathbf{u} \cdot \nabla \mathbf{u}$ and $\nu \nabla^2 \mathbf{u}$, respectively. Here, \mathbf{u} is the velocity and ν is the kinematic viscosity. Throughout the remainder of this review, we define the Reynolds number as

$$\text{Re} = u_{\text{rms}} / \nu k_f, \quad (9)$$

where $u_{\text{rms}} = \langle \mathbf{u}^2 \rangle^{1/2}$ is the rms velocity within some appropriate volume and k_f is the wavenumber of the energy-carrying eddies, which is also known as the integral or correlation wavenumber. It can be defined through a weighted average of the inverse wavenumber over the kinetic energy spectrum, $E_K(k, t)$, where $k = |\mathbf{k}|$ is the modulus of the wave vector \mathbf{k} , and t is time. The kinetic energy spectrum is normalized such that

$$\int_0^\infty E_K(k, t) dk = \frac{1}{2} \rho_0 \langle \mathbf{u}^2 \rangle, \quad (10)$$

where $\rho_0 = \langle \rho \rangle$ is the volume average of the gas density ρ . For incompressible and weakly compressible flows, it is customary to ignore fluctuations of ρ in the definition of $E_K(k, t)$. In fact, there is no unique way of incorporating density. For supersonic turbulence, this is very much a current research topic in its own right. We refer here to the papers of Kritsuk et al. (2007), Galtier and Banerjee (2011), and Banerjee and Galtier (2013).

Returning to the case of incompressible or weakly compressible (subsonic) turbulence, a formal definition of k_f can be written as

$$k_f^{-1} = \int k^{-1} E_K(k, t) dk \bigg/ \int E_K(k, t) dk. \quad (11)$$

Note that $k_f = k_f(t)$ is in general time-dependent, which can be important in studies of decaying turbulence. An important example is helical MHD turbulence, because it drives an inverse cascade which manifests itself in a time-dependent decrease of $k_f(t)$; see Tevzadze et al. (2012) and Kahniashvili et al. (2013) for recent examples. In most of the cases considered below we consider a time average of k_f .

MHD turbulence is additionally characterized by the *magnetic* Reynolds number,

$$\text{Re}_M = u_{\text{rms}} / \eta k_f, \quad (12)$$

where η is the magnetic diffusivity. The ratio $\text{Re}_M/\text{Re} = \nu/\eta = \text{Pr}_M$ is the magnetic Prandtl number. Furthermore, a magnetic energy spectrum $E_M(k, t)$ can be defined such that

$$\int_0^\infty E_M(k, t) dk = \frac{1}{2} \mu_0^{-1} \langle \mathbf{B}^2 \rangle, \quad (13)$$

where \mathbf{B} is the magnetic field and μ_0 is the vacuum permeability. Analogously to Equation (11) we can then also define a magnetic correlation wavenumber $k_M(t)$. The relative alignment between \mathbf{u} and \mathbf{B} is characterized by the so-called cross helicity, $\langle \mathbf{u} \cdot \mathbf{B} \rangle$, and its scale dependence is characterized by the cross helicity spectrum $E_C(k, t)$ with the normalization $\int E_C(k, t) dk = \langle \mathbf{u} \cdot \mathbf{B} \rangle$. This quantity is a pseudoscalar and changes sign for a mirror-reflected image of the turbulence. Other important helicities are the kinetic helicity, $\langle \mathbf{w} \cdot \mathbf{u} \rangle$, with $\mathbf{w} = \nabla \times \mathbf{u}$ being the vorticity, the current helicity, $\langle \mathbf{J} \cdot \mathbf{B} \rangle$, with $\mathbf{J} = \nabla \times \mathbf{B}/\mu_0$ being the current density, and, in particular, the magnetic helicity, $\langle \mathbf{A} \cdot \mathbf{B} \rangle$, with \mathbf{A} being the magnetic vector potential such that $\mathbf{B} = \nabla \times \mathbf{A}$.

In some cases we also discuss the evolution of a passive scalar, whose concentration is governed by a corresponding diffusivity κ . The relevant non-dimensional parameter is the Péclet number, $\text{Pe} = u_{\text{rms}}/\kappa k_f$.

5.2 Dynamo instability and spectrum

In the absence of an imposed magnetic field, the zero-field limit is unstable to dynamo action when the magnetic Reynolds number exceeds a critical value,

$$\text{Re}_M > \text{Re}_{M,\text{crit}} \quad (\text{dynamo instability}). \quad (14)$$

In practice, this means that the theory of Kolmogorov turbulence is not directly applicable to most astrophysical flows when the gas is ionized and therefore electrically conducting.

In this section we restrict ourselves to non-helical isotropic turbulence, i.e., $\langle \mathbf{w} \cdot \mathbf{u} \rangle \ll k_f \langle \mathbf{u}^2 \rangle$. In that case, only random or turbulent magnetic fields can be expected. This possibility was already anticipated by Batchelor (1950), but the relevant theory was only developed later by Kazantsev (1968). He assumed that the velocity field was given by a smooth large-scale random flow and found that the resulting magnetic field has typical wavenumbers close to the resistive cutoff wavenumber, $k_\eta = \langle \mu_0^2 \mathbf{J}^2 / \eta^2 \rangle^{1/4}$, and much larger than k_f . In fact, his work predicted a $k^{3/2}$ spectrum for the magnetic field in the wavenumber range $k_f < k < k_\eta$.

The first numerical solutions of such dynamos have been performed by Meneguzzi et al. (1981) at a resolution of just 64^3 collocation points. Those were the “golden years” of numerical turbulence research. For the first time, many of the ideas in turbulence could be put to the test and, although the numerical resolution was still poor, it was clear that it could only be a matter of time until all the newly emerging results will be confirmed at better resolution.

In the following years, small-scale dynamo action emerged in several direct numerical simulations (DNS). At first it appeared that kinetic helicity had only a minor effect in Cartesian simulations (Meneguzzi and Pouquet 1989; Kida et al. 1991; Nordlund et al. 1992). This was later understood to be an artefact of the lack of scale separation, i.e., k_f/k_1 was not big enough (Haugen et al. 2004a). Meanwhile, global convection simulations in spherical shells did produce large-scale magnetic fields (Gilman 1983; Glatzmaier 1985). Remarkably, although there was general awareness of the concepts of large-scale and small-scale

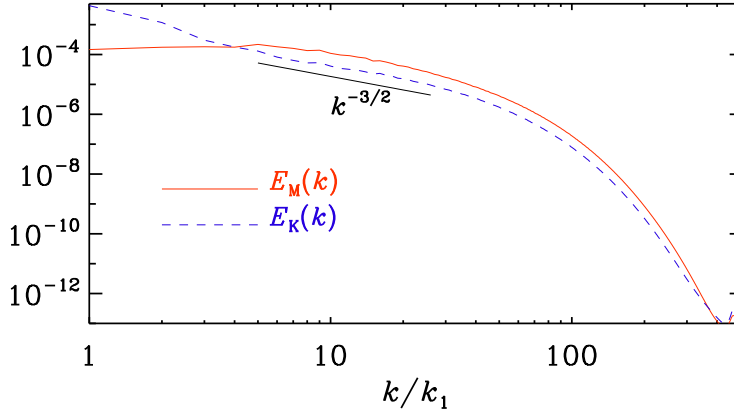


Fig. 7 Magnetic, kinetic and total energy spectra. $\text{Re} = \text{Re}_M = 960$ using 1024^3 meshpoints. Courtesy of Nils Erland Haugen (Haugen et al. 2003).

dynamoes, which was also clearly spelled out in an early review of Vainshtein and Zeldovich (1972), the theory of Kazantsev (1968) was still not yet widely cited in the West. This has changed by the late 1990s (e.g., Gruzinov et al. 1996; Subramanian 1998; Kulsrud 1999), and by the early 2000s many groups investigated the small-scale dynamo systematically (Cho and Vishniac 2000; Schekochihin et al. 2002, 2004a, 2004b; Haugen et al. 2003, 2004a).

Although the resolution has improved significantly over the past two decades, some important aspects of small-scale dynamos was evident already early on. In particular, Meneguzzi et al. (1981) and Kida et al. (1991) found that the magnetic energy spectrum reaches a maximum at a wavenumber k_M that is by a factor of ≈ 6 larger than k_f , which is where the kinetic energy has its maximum. This was an aspect that was later motivated by the work of Subramanian (1998), who proposed that k_M/k_f should be of the order of $\text{Re}_{M,\text{crit}}^{1/2}$. This result was indeed borne out by all the DNS obtained so far. In Figure 7 we reproduce the result of Haugen et al. (2003) using 1024^3 meshpoints. For larger values of Pr_M , $\text{Re}_{M,\text{crit}}$ increases, so k_M also increases, making it harder to confirm the expected scaling in that regime. Indeed, Schekochihin et al. (2004b) propose that at large values of Pr_M the field shows folded structures. While Brandenburg and Subramanian (2005) confirmed the presence of folded structures in a simulation with $\text{Pr}_M = 50$, they found them rather the exception and showed other cases where the field was not folded. Recent simulations by Bhat and Subramanian (2013) confirmed that, after sufficiently many turnover times, k_M/k_f is of the order of $\text{Re}_{M,\text{crit}}^{1/2}$ even when $\text{Pr}_M = 50$.

Note that, at the position where the magnetic energy spectrum peaks, the magnetic field is in super-equipartition with the kinetic energy by a factor of 2–3. Initially, this was a somewhat surprising result in view of the work of GS95, according to which one might have expected equipartition. Subsequent work using large eddy simulations suggested that this super-equipartition would not persist deeper into the inertial range, provided Re and Re_M are large enough. Indeed, a trend toward equipartition can be seen in the compensated energy spectra of Haugen and Brandenburg (2006); see also Figure 8, where a Smagorinsky subgrid

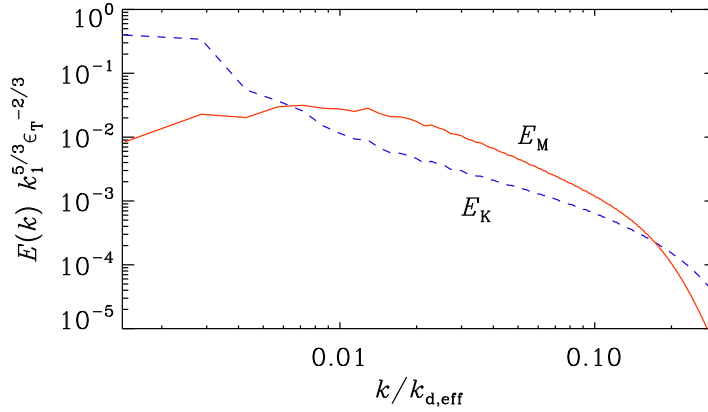


Fig. 8 Magnetic and kinetic energy spectra for runs with 512^3 meshpoints and hyperviscosity with hyper-resistivity (solid line) and Smagorinsky viscosity with hyperresistivity (red, dashed line). Note the mutual approach of kinetic and magnetic energy spectra before entering the dissipative subrange. Adapted from Haugen and Brandenburg (2006).

scale model was used for the momentum equation and hyper-resistivity in the induction equation.

5.3 Small-scale dynamo action at small values of Pr_M

The question of what happens in the case of $\text{Pr}_M \ll 1$ has always been on people's mind. Small values of Pr_M are characteristic of denser bodies such as stars, planets, and especially liquid metals. Only in recent years a clearer picture has emerged of what happens in the limit $\text{Pr}_M \rightarrow 0$. By comparing the onset of dynamo action, it became clear that $\text{Re}_{M,\text{crit}}$ grew larger and larger as one approached the value $\text{Pr}_M = 0.1$ (Schekochihin et al. 2005). Crucial insight was gained through a paper by Iskakov et al. (2007), who found that $\text{Re}_{M,\text{crit}}$ has a local maximum at $\text{Pr}_M = 0.1$, and that it decreases again as Pr_M is decreased further. Early work of Rogachevskii and Kleeorin (1997) did already predict an increased value of $\text{Re}_{M,\text{crit}}$ in the limit of small values of Pr_M , but not really a local maximum. Boldyrev and Cattaneo (2004) argue that the reason for an increased value of $\text{Re}_{M,\text{crit}}$ is connected with the “roughness” of the velocity field, as quantified by the scaling exponent ζ in velocity differences $\delta u_\ell \sim \ell^\zeta$ over spatial separations ℓ . In the diffusive subrange, $\zeta = 1$, so the velocity is smooth, but in the inertial range we have $\zeta \approx 0.4$, so velocity gradients diverge and the velocity field is therefore called “rough.”

The connection with roughness also helped explaining the occurrence of a maximum in $\text{Re}_{M,\text{crit}}$ as Pr_M goes through 0.1. Indeed, the reason for this is that near $\text{Pr}_M = 0.1$ the resistive wavenumber is about 10 times smaller than the viscous one and thus right within the “bottleneck” where the spectrum is even shallower than in the rest of the inertial range, with a local scaling exponent $\zeta \rightarrow 0$, corresponding to turbulence that is in this regime rougher still, explaining thus the apparent divergence of $\text{Re}_{M,\text{crit}}$.

The physical reality of the bottleneck effect remains still a matter of debate, but the work of Falkovich (1994) suggests that it is related to the fact that near the viscous cut-off wavenumber the flow becomes harder to stir, and that triangle interactions between a

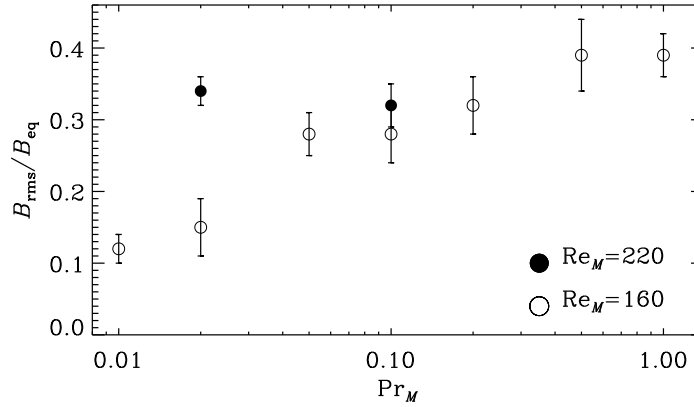


Fig. 9 Saturation field strengths for small-scale dynamos as a function of Pr_M for two values of Re_M . Note that for $Re_M = 160$ (open symbols) the dynamo is close to onset and the saturation field strength declines with decreasing values of Pr_M , while for $Re_M = 220$ (filled symbols) the field strength changes only weakly although only two data points are available.

wavenumber in the bottleneck range with wavenumbers in the dissipative subrange experience a difficulty in disposing of their energy. It is claimed in Beresnyak and Lazarian (2010) that the MHD turbulence while formally local, is more diffusive in terms of the interactions involved. This property termed "diffuse locality", may explain that the bottleneck effect in hydrodynamics is much more prominent than in MHD. Thus, one may suspect that even the highest resolution simulations would still not be showing the actual inertial range, but are influenced by an extended bottleneck effect Beresnyak and Lazarian (2009). This may be the reason why the numerically measured spectrum is a bit shallower than the GS95 prediction. A numerical study in Beresnyak (2011) seems to support this conclusion.

It has recently become possible to demonstrate that in the nonlinear regime, when the magnetic field affects the flow, the hydrodynamic bottleneck effect tends to be suppressed as the field strength becomes appreciable, so the divergence in the roughness disappears and there is a smooth dependence of the saturation field strength on the value of Pr_M ; see Brandenburg (2011) for details. In Figure 9 we show the saturation energy of small-scale dynamos as a function of Pr_M using the data of Tables 1 and 2 of Brandenburg (2011). It is clear that the position $Pr_M = 0.1$ is no longer special and that dynamo action is possible for small values of Pr_M as well. For $Re_M = 160$ the value of B_{rms}/B_{eq} is still Re_M -dependent, but this may be an artefact of the dynamo being close to onset. For $Re_M = 220$ the dynamo is more clearly supercritical and, although there are only two data points, the results are now more clearly consistent with B_{rms}/B_{eq} being independent of Re_M .

5.4 Helically driven turbulence

Eigenfunctions of the curl operator provide an ideal means of stirring the flow. In wavenumber space, these take the form (Haugen et al. 2004a)

$$\mathbf{f}_k = \mathbf{R} \cdot \mathbf{f}_k^{(nohel)} \quad \text{with} \quad R_{ij} = \frac{\delta_{ij} - i\sigma\epsilon_{ijk}\hat{k}_k}{\sqrt{1 + \sigma^2}}, \quad (15)$$

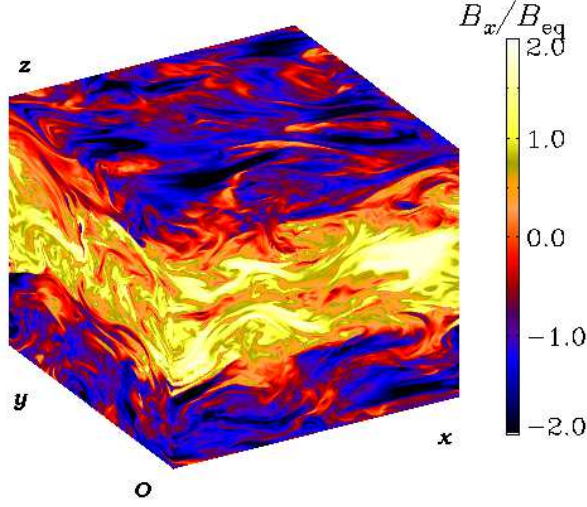


Fig. 10 Visualization of B_x on the periphery of the computational domain for a run with $\text{Re}_M = 600$ and a resolution of 512^3 mesh points. Note the clear anisotropy with structures elongated in the direction of the field (which lies in the xy plane). Adapted from Brandenburg et al. (2008a).

where σ is a measure of the helicity of the forcing and $\sigma = 1$ for positive maximum helicity of the forcing function. Furthermore,

$$\mathbf{f}_k^{(\text{nohel})} = (\mathbf{k} \times \hat{\mathbf{e}}) / \sqrt{k^2 - (\mathbf{k} \cdot \hat{\mathbf{e}})^2} \quad (16)$$

is a non-helical forcing function, where $\hat{\mathbf{e}}$ is an arbitrary unit vector not aligned with \mathbf{k} ; note that $|\mathbf{f}_k|^2 = 1$ and $\mathbf{f}_k \cdot (i\mathbf{k} \times \mathbf{f}_k)^* = 2\sigma k / (1 + \sigma^2)$, so the relative helicity of the forcing function in real space is $2\sigma / (1 + \sigma^2)$. When $\sigma = 0$, the forcing function is non-helical, and so is the resulting flow. This case is special, as was demonstrated on various occasions. Firstly, helical turbulence introduces an α effect which means that a weak *large-scale* magnetic field becomes destabilized and will be amplified. In Figure 10 we show a visualization of one of the field components on the periphery of a Cartesian domain with periodic boundary conditions. Note the presence of both large-scale and small-scale components. Secondly, in the absence of forcing, a fully helical magnetic field decays more slowly than a non-helical one. Specifically, we have (Biskamp and Müller 1999; Biskamp 2003)

$$\langle \mathbf{B}^2 \rangle(t) = \frac{\langle \mathbf{B}^2 \rangle(0)}{(1 + t/\tau)^{2/3}}, \quad (17)$$

where $\tau = \sqrt{\mu_0 \rho_0} \langle \mathbf{A} \cdot \mathbf{B} \rangle / \langle \mathbf{B}^2 \rangle^{3/2}$ is the typical decay time scale. In Figure 11 we compare results of two simulations of Kahniashvili et al. (2013), one with an initial magnetic helicity and the other one without. Note the slower decay proportional to $t^{-2/3}$ in the helical case compared to the faster t^{-1} decay in the non-helical case. In both cases, time has been normalized by $\tau = \sqrt{\mu_0 \rho_0} / k_{f0} B_{\text{rms}}$, where $k_{f0} = k_f(t = 0) \approx 15k_1$. The rms velocity is about 20% of the B_{rms} in the helical case and about 28% in the non-helical case. The Reynolds number based on $k_f(t)$, which decreases with time either like $t^{-2/3}$ in the helical

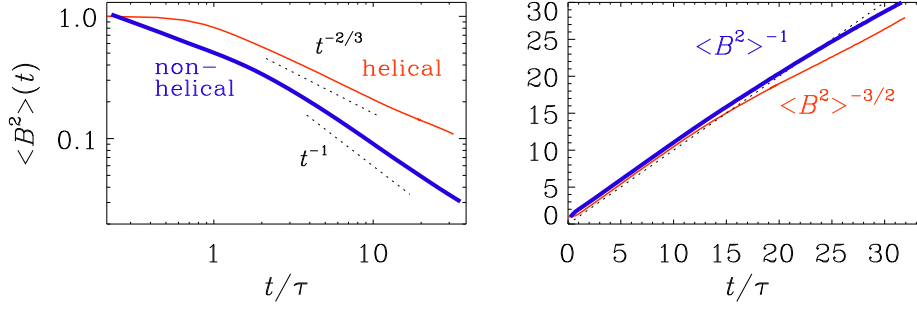


Fig. 11 Decay of magnetic energy with and without initial helicity (left) and the approximately linear evolution of $\langle B^2 \rangle^{-3/2}$ and $\langle B^2 \rangle^{-1}$ in the two cases (right).

case, or like $t^{-1/2}$ in the non-helical case, increases from 50 to 100 during the course of both simulations. Even if the magnetic field is initially not fully helical, the relative helicity will increase, because magnetic energy decays faster than magnetic helicity; see Tevzadze et al. (2012). These considerations are important for primordial magnetic fields generated during cosmological phase transitions, because the inverse cascade allow the fields to reach appreciable length scales at the present time (Brandenburg et al. 1996; Banerjee and Jedamzik 2004; Kahnishvili et al. 2010).

The α effect is the reason behind the large-scale dynamo effect leading to the global magnetic field observed in many astrophysical bodies (Moffatt 1978; Parker 1979; Krause and Rädler 1980). The resulting magnetic field is helical and its helicity has the same sign as α . However, because of total magnetic helicity conservation, no net magnetic helicity can be produced. Therefore the α effect produces magnetic helicity of opposite signs at large and small length scales at the same time. In Figure 12 we show magnetic and kinetic energy spectra compensated by $k^{1.5}$ together with compensated magnetic and kinetic helicity spectra, normalized by $k/2$ and $1/2k$, respectively. This normalization allows us to see whether or not the realizability conditions, $E_M(k) \geq 2kH_M(k)$ and $E_K(k) \geq 2H_K(k)/k$, are close to being saturated. Note also that $H_M(k)$ changes sign and becomes negative at $k/k_1 = 1$ (thin line), and is positive at all larger values of k/k_1 (thick line).

The case of homogeneous helical turbulence is a particularly interesting example, because accurate estimates can be made about the saturation field strength and the magnetic helicity balance, for example. However, such circumstances are not usually found in realistic applications. The significance of homogeneity is that then the divergence of the magnetic helicity fluxes vanishes and does not affect the magnetic helicity evolution, so we have

$$\frac{d}{dt} \langle \mathbf{A} \cdot \mathbf{B} \rangle = -2\eta\mu_0 \langle \mathbf{J} \cdot \mathbf{B} \rangle. \quad (18)$$

Furthermore, in a homogeneous system, $\langle \mathbf{A} \cdot \mathbf{B} \rangle$ is gauge-invariant, so in the steady state we have

$$\langle \mathbf{J} \cdot \mathbf{B} \rangle = 0 \quad (\text{steady state}). \quad (19)$$

This is remarkable and applies even (and especially) in the case of helical forcing when large-scale fields can be generated by the α effect.

For the rest of this review, it will be crucial to distinguish between large-scale and small-scale magnetic fields. We do this by making use of the following decomposition:

$$\mathbf{U} = \overline{\mathbf{U}} + \mathbf{u}, \quad \mathbf{B} = \overline{\mathbf{B}} + \mathbf{b}. \quad (20)$$

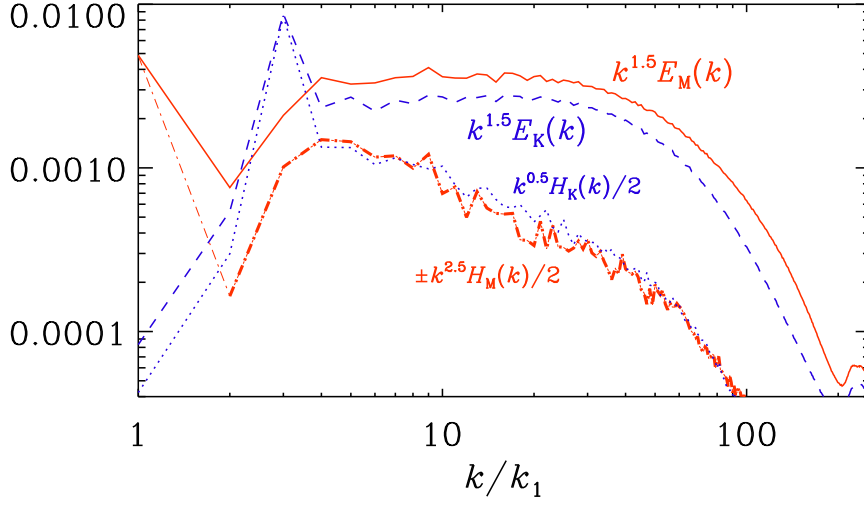


Fig. 12 Compensated time-averaged spectra of kinetic and magnetic energy (dashed and solid lines, respectively), as well as of kinetic and magnetic helicity (dotted and dash-dotted lines, respectively), for a run with $\text{Re}_M \approx 600$. Note that $H_M(k)$ changes sign and becomes negative $k/k_1 = 1$ (indicated by a thin line), and is positive at all larger values of k/k_1 (indicated by a thicker line). Adapted from Brandenburg et al. (2008a), where however $H_K(k)$ and $H_M(k)$ are compensated by $k^{1.2}$ and $k^{3.2}$, respectively.

In the previous sections of this review, there was no mean flow, so $\mathbf{U} = \mathbf{u}$, but from now on we shall denote the full velocity by a capital letter. Likewise, the vorticity of \mathbf{U} is given by $\mathbf{W} = \nabla \times \mathbf{U}$.

In rotating astrophysical bodies, a commonly used average is the azimuthal one. However, in the present case of fully periodic Cartesian domains, the resulting large-scale fields can be described by planar averages, such as xy , yz , or xz averages. The resulting mean fields, $\overline{\mathbf{B}}$, depend then still on z , x , or y , in addition to t . Examples of such fields are those proportional to $(\sin kz, \cos kz, 0)$, $(0, \sin kx, \cos kx)$, and $(\cos ky, 0, \sin ky)$, respectively. All these examples obey

$$\nabla \times \overline{\mathbf{B}} = k \overline{\mathbf{B}} \quad (21)$$

and are thus eigenfunctions of the curl operator with eigenvalue k . In particular, it follows then that $\overline{\mathbf{J}} \cdot \overline{\mathbf{B}} = k \overline{\mathbf{B}}^2 / \mu_0$ is uniform. This can only be compatible with Equation (19), if there is a residual (small-scale or fluctuating) magnetic field, $\mathbf{b} = \mathbf{B} - \overline{\mathbf{B}}$, which obeys $\langle \mathbf{j} \cdot \mathbf{b} \rangle = -\langle \overline{\mathbf{J}} \cdot \overline{\mathbf{B}} \rangle$. Here, $\mathbf{j} = \nabla \times \mathbf{b} / \mu_0$ is the corresponding current density. Assuming $\langle \mathbf{j} \cdot \mathbf{b} \rangle = \epsilon_f k_f \langle \mathbf{b}^2 \rangle / \mu_0$, we find that $\overline{\mathbf{B}}^2 / \langle \mathbf{b}^2 \rangle = \epsilon_f k_f / k$, which can exceed unity in cases of fully helical forcing ($\epsilon_f \rightarrow \pm 1$). We recall that the parameter ϵ_f is related to the helicity parameter σ in the forcing function (15) via $\epsilon_f = 2\sigma / (1 + \sigma^2)$. Repeating this calculation for the late saturation phase of a dynamo, we have

$$\frac{\overline{\mathbf{B}}^2}{\langle \mathbf{b}^2 \rangle} \approx \frac{\epsilon_f k_f}{k} \left[1 - e^{-2\eta k^2 (t - t_{\text{sat}})} \right], \quad (22)$$

with a suitable integration constant t_{sat} , having to do with just properties of the initial field strength. This equation describes the late ($t > t_{\text{sat}}$), resistively dominated saturation phase of a helically driven dynamo of α^2 type. By differentiating this equation again, we can find

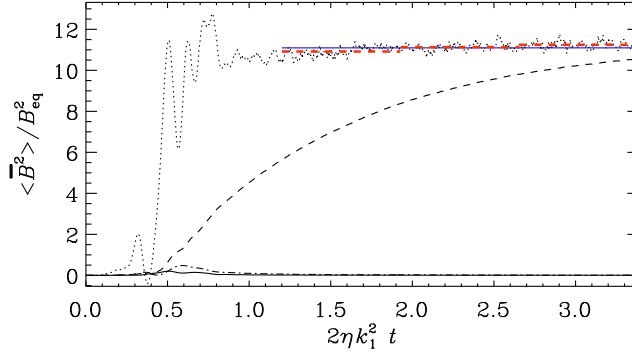


Fig. 13 Example showing the evolution of the normalized $\langle \overline{B}^2 \rangle$ (dashed) and that of $\langle \overline{B}^2 \rangle + d\langle \overline{B}^2 \rangle / d(2\eta k_1^2 t)$ (dotted), compared with its average in the interval $1.2 \leq 2\eta k_1^2 t \leq 3.5$ (horizontal blue solid line), as well as averages over 3 subintervals (horizontal red dashed lines). Here, \overline{B} is evaluated as an xz average, $\langle B \rangle_{xz}$. For comparison we also show the other two averages, $\langle B \rangle_{xy}$ (solid) and $\langle B \rangle_{yz}$ (dash-dotted), but their values are very small. Adapted from Candelaresi and Brandenburg (2013).

that the final saturation field strength, $\overline{B}_{\text{sat}} = \overline{B}_{\text{rms}}(t \rightarrow \infty)$, obeys (Candelaresi and Brandenburg 2013)

$$\overline{B}_{\text{sat}}^2 \approx \overline{B}^2 + d\overline{B}^2 / d(2\eta k_1^2 t). \quad (23)$$

This equation allows one to compute the value of $\overline{B}_{\text{sat}}$ based on the measured rate at which \overline{B}^2 increases. It is now routinely used to estimate $\overline{B}_{\text{sat}}$ without actually reaching the final state; see Figure 13 for an example.

5.5 Turbulent mixing and non-diffusive transport

Turbulent flows are known to be capable of enhanced mixing. A prime example is the mixing of a passive scalar concentration $C(\mathbf{x}, t)$, whose evolution is governed by the equation

$$\frac{\partial C}{\partial t} = -\nabla \cdot (UC) + \kappa \nabla^2 C. \quad (24)$$

Loosely speaking, turbulent mixing can be modeled as an enhanced diffusivity in the corresponding evolution equation for the *mean* passive scalar concentration $\overline{C}(\mathbf{x}, t)$, which then takes the form

$$\frac{\partial \overline{C}}{\partial t} = -\nabla \cdot (\overline{U}\overline{C}) + \kappa_T \nabla^2 \overline{C}, \quad (25)$$

where $\kappa_T = \kappa + \kappa_t$ is the sum of molecular (or atomic) and turbulent diffusivities.

In a more precise formulation, κ_t becomes not only a tensor, κ_{ij} , but also an integral kernel that takes into account that on the right-hand side of Equation (25) higher-order derivatives of \overline{C} in space and time appear. In particular, there can in principle also be a term of the form $\nabla \cdot (\gamma^C \overline{C})$ on the right-hand side which describes turbulent pumping or turbophoresis, and γ^C is a vector. This term acts like advection, but without any material motion. (In a kernel formulation, such a term could in principle be subsumed into the integral kernel.) However, under isotropic conditions, γ^C must vanish and the diffusivity tensor κ_{ij} becomes an isotropic tensor $\kappa_t \delta_{ij}$. Analogous equations can also be derived for the magnetic induction equation and the momentum equation. In both cases this can lead to physically new

effects such as the mean-field (or large-scale) dynamo instability and the negative effective magnetic pressure instability (NEMPI), which will be discussed further below. The former exists in isotropic turbulence, while the latter requires inhomogeneity and sufficiently strong density stratification.

In the simulations presented in Section 5.4 we found the development of large-scale fields of Beltrami type. Such fields do indeed emerge as eigenfunctions of the related mean-field induction equation with constant coefficients,

$$\frac{\partial \overline{\mathbf{B}}}{\partial t} = \nabla \times (\overline{\mathbf{U}} \times \overline{\mathbf{B}} + \alpha \overline{\mathbf{B}} - \eta_T \mu_0 \overline{\mathbf{J}}). \quad (26)$$

Significant progress in this field has recently become possible through the numerical determination of the full set of turbulent transport coefficients. This method is known as the test-field method and involves the solution of additional evolution equations for the magnetic fluctuations arising from a given test field. One needs enough test fields to obtain all tensor components. By allowing the test fields to attain suitable variability in space and time, it is possible to determine then also the full integral kernel in spectral space.

The results obtained so far have shown that

$$\alpha \approx \alpha_0 \equiv -\epsilon_f u_{\text{rms}}/3 \quad (27)$$

and

$$\eta_t \approx \eta_{t0} \equiv u_{\text{rms}}/3k_f \quad (28)$$

for $\text{Re}_M \gtrsim 1$. For $\text{Re}_M \lesssim 1$, both coefficients increase linearly with increasing Re_M (Sur et al. 2008). In the nonlinear regime, there can also be velocity fluctuations generated through the presence of a mean field, but this requires what is known as magnetic background turbulence, i.e., magnetic fluctuations that would be present even without a mean magnetic field. This is in principle possible when there is small-scale dynamo action. This case can be treated with a correspondingly modified test-field method (Rheinhardt and Brandenburg 2010).

In the following we state several important results obtained by using the test-field method. We did already mention that for fully helical turbulence and large values of Re_M , α and η_t attain values of the order of $\pm u_{\text{rms}}/3$ and $u_{\text{rms}}/3k_f$, respectively. In turbulence, both coefficients possess a wavenumber dependence that is of the form of a Lorentzian proportional to $(1 + k^2/k_f^2)^{-1}$, corresponding to an exponential integral kernel proportional to $\exp[-(z - z')k_f]$; see Brandenburg et al. (2008b). When the mean field is non-steady, the memory effect can become important and this leads to a dependence of the form $(1 - i\omega\tau)^{-1}$, corresponding to a kernel proportional to $\exp(-|t - t'|/\tau)$ for $t' < t$, and 0 otherwise. Here, $\tau \approx (u_{\text{rms}}k_f)^{-1}$ is the correlation time.

In the limit $\ell = 1/k_f \rightarrow 0$ and $\tau \rightarrow 0$, the integral kernels become δ functions in space and time. However, this approximation breaks down at the bottom of the solar convection zone, where the resulting mean magnetic field in dynamo models often shows structures on scales much smaller than ℓ (Chatterjee et al. 2011). Furthermore, nonlocality in time is violated when the mean magnetic field is either growing or decaying. Ignoring this can lead to discrepancies that are well detectable with the test-field method (Hubbard and Brandenburg 2009; Rädler et al. 2011). Finally, when the mean magnetic field depends strongly on both space and time, the integral kernel in spectral space becomes approximately proportional to $(1 - i\omega\tau + \ell^2 k^2)^{-1}$. This form has the advantage that it can easily be treated in real space by solving an evolution equation in time with a positive diffusion term, i.e.,

$$\left(1 + \tau \frac{\partial}{\partial t} - \ell^2 \nabla^2\right) \overline{\mathcal{E}}_i = \alpha_{ij} \overline{B}_j + \eta_{ijk} \overline{B}_{j,k}. \quad (29)$$

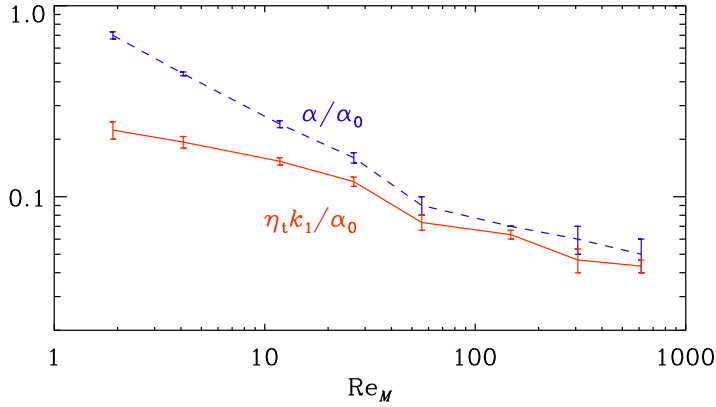


Fig. 14 Re_M -dependence of α and $\tilde{\eta}_t$. Both curves are normalized by α_0 . Adapted from Brandenburg et al. (2008a).

Here, α_{ij} and η_{ijk} are the usual α effect and turbulent diffusivity tensors for $\omega \rightarrow 0$ and $k \rightarrow 0$, and equal to $\alpha\delta_{ij}$ to $\eta_t\epsilon_{ijk}$ in the isotropic case. This equation has been studied in some detail by Rheinhardt and Brandenburg (2012). It is a special form of the telegraph equation, which has been studied in similar contexts (Brandenburg et al. 2004; Chamandy et al. 2013).

Using the quasi-kinematic test-field method, Brandenburg et al. (2008a) showed that in the case of a saturated dynamo, both α and η_t remain weakly Re_M -dependent; see Figure 14. Note that no fully asymptotic regime has been obtained yet, so it remains unclear when or whether this will happen. It is clear, however, that α must approach $\eta_t k_1$ at large Re_M for the system to be in the stationary saturated state. However, in view of the astrophysical importance of turbulent dissipation, the remaining weak dependence of η_t on Re_M is expected to disappear eventually.

6 Inhomogeneous MHD turbulence

6.1 Density stratification

Stratification refers to nonuniformity that is usually caused by gravity. As a consequence, pressure increases in the direction of the gravity, and this causes similar changes in density and/or temperature. The turbulence intensity can itself also be stratified. This usually comes as a consequence of density stratification, but one can envisage circumstances in which the forcing is nonuniform. Such non-uniformity affects turbulent transport—not just diffusive but also non-diffusive transport, similar to the pumping velocity proportional to γ^C , described in Section 5.5. Both effects are astrophysically important. Stratification usually leads to a suppression of diffusive transport. An example is shown in Figure 15, where we show the suppression of the vertical passive scalar diffusivity as a function of the stratification, which is here measured by the normalized Brunt–Väisälä frequency, N , with $N^2 = -\mathbf{g} \cdot \nabla s / c_p$ and s being the specific entropy. For details of this, see the work of Kitchatinov and Brandenburg (2012).

Suppression of turbulent transport, for example, is critical for understanding the depletion of primordial elements (e.g., lithium) by mixing with deeper layers in the stably stratified lower overshoot layer of the convection zones of stars with outer convection zones. The

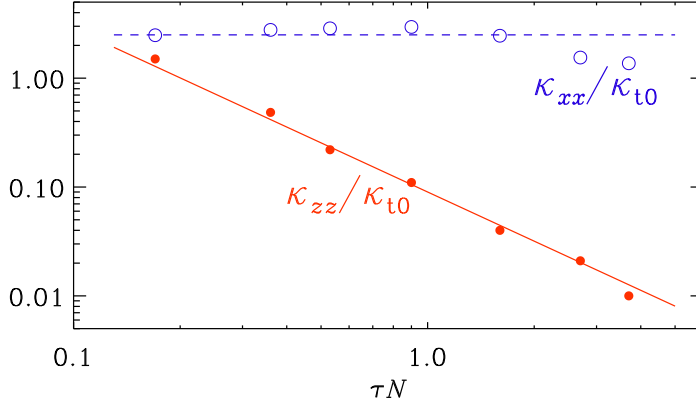


Fig. 15 Dependence of κ_{xx}/κ_{t0} (open symbols) and κ_{zz}/κ_{t0} (filled symbols) on the normalized buoyancy frequency. The dashed line shows that $\kappa_{xx}/\kappa_{t0} \approx 2.5$ while the solid line gives $\kappa_{zz}/\kappa_{t0} \approx 0.09 (\tau N)^{-3/2}$. Adapted from Kitchatinov and Brandenburg (2012).

suppression is here caused mainly by the stabilizing entropy gradient [reversing the gradient of s leads the negative values of N , corresponding the onset of convection with exponential growth proportional to $\exp(\text{Im} N t)$.] In the following, we shall focus on another manifestation of stratification, namely the expansion of rising structures as they ascent into less dense surroundings. For that purpose, we make the assumption of an isothermal equation of state, which is a simplification that leads to a constant pressure scale height and suppresses also the stabilizing effect from the entropy gradient. For further discussion on this, see the papers by Brandenburg et al. (2012a) and Käpylä et al. (2012) in the context of NEMPI; see Section 5.5.

6.2 Stratified turbulence with a vertical field

In the presence of stratification and an imposed magnetic field along the direction of stratification, there is the possibility of producing another pseudoscalar called cross helicity. On theoretical grounds, one expects (Rüdiger et al. 2011)

$$\langle \mathbf{u} \cdot \mathbf{b} \rangle \propto g \overline{B}. \quad (30)$$

More specifically, it turns out that

$$\langle \mathbf{u} \cdot \mathbf{b} \rangle = -\eta_t \overline{B} / H_\rho, \quad (31)$$

where H_ρ is the density scale height. This does indeed turn out to be the case, as has been shown using simulations of forced isothermal turbulence in the presence of gravity. The result is shown in Figure 16, where we plot $\langle \mathbf{u} \cdot \mathbf{b} \rangle$ as a function of Re_M .

6.3 Effects of rotation

In the presence of stratification and/or rotation, MHD turbulence is subject to a range of new effects. These phenomena are associated with the vectors \mathbf{g} (gravity) and $\boldsymbol{\Omega}$ (angular velocity), which introduce preferred directions to the flow. They do so in different ways, because

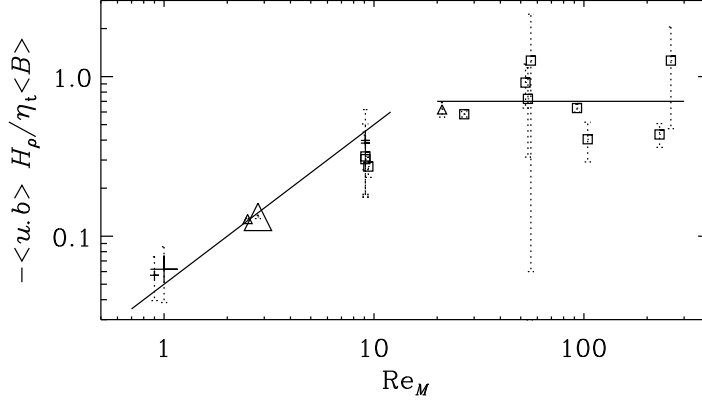


Fig. 16 Dependence of the normalized cross helicity on Re_M for various field strength $B_z/B_{\text{eq}} < 0.1$, $\text{Pm} = 1$, $k_f/k_1 = 2.2$, and $H_\rho k_1 = 2.5$. The straight line denotes the fit $\langle \mathbf{u} \cdot \mathbf{b} \rangle / \tau g \langle B \rangle = 0.05 \text{Re}_M$.

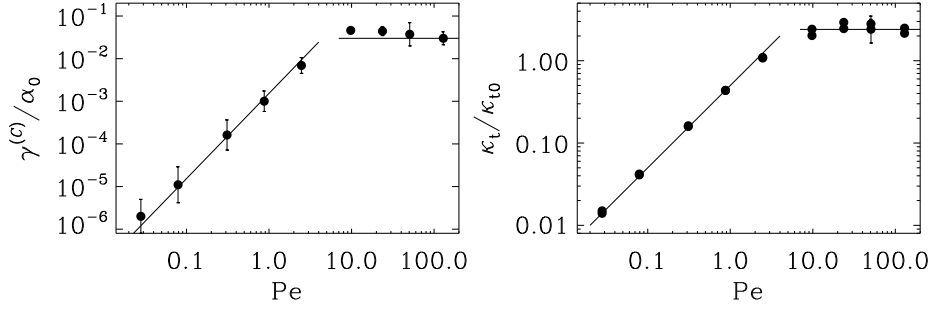


Fig. 17 Dependence of passive scalar pumping velocity, $\gamma^{(C)}$, and passive scalar diffusivity κ_t on Peclet number, Pe . The scale separation ratio is $k_f/k_1 = 5$.

\mathbf{g} is a polar vector (identical to its mirror image) while $\boldsymbol{\Omega}$ is an axial vector (antiparallel to its mirror image). This means that turbulent transport effects characterized by some effective velocity must be proportional to another polar vector. This can then either be the vector \mathbf{g} or, in forced turbulence simulations, where it is possible to produce helical turbulence, it can be the vector $\hat{\boldsymbol{\Omega}}$. In that case there is kinetic helicity, $\langle \mathbf{w} \cdot \mathbf{u} \rangle$, which is a pseudoscalar, so $\langle \mathbf{w} \cdot \mathbf{u} \rangle \boldsymbol{\Omega}$ would also be a polar vector, allowing pumping even in the homogeneous case if there is rotation and helicity.

In Figure 17 we show such an example, where there is fully helical turbulence that is initially isotropic, but because of rotation it becomes anisotropic and there is now a polar vector that leads to turbulent pumping with the velocity

$$\gamma^{(C)} \approx 0.075 \langle \mathbf{w} \cdot \mathbf{u} \rangle \boldsymbol{\Omega} / (u_{\text{rms}} k_f)^2. \quad (32)$$

A similar result has previously been obtained by Pipin (2008) and Mitra et al. (2009) for shear flows, where the resulting mean vorticity vector acts as the relevant pseudovector. However, these situations are somewhat artificial, because helicity does not normally occur in the absence of additional stratification, so any pumping would still be indirectly associated

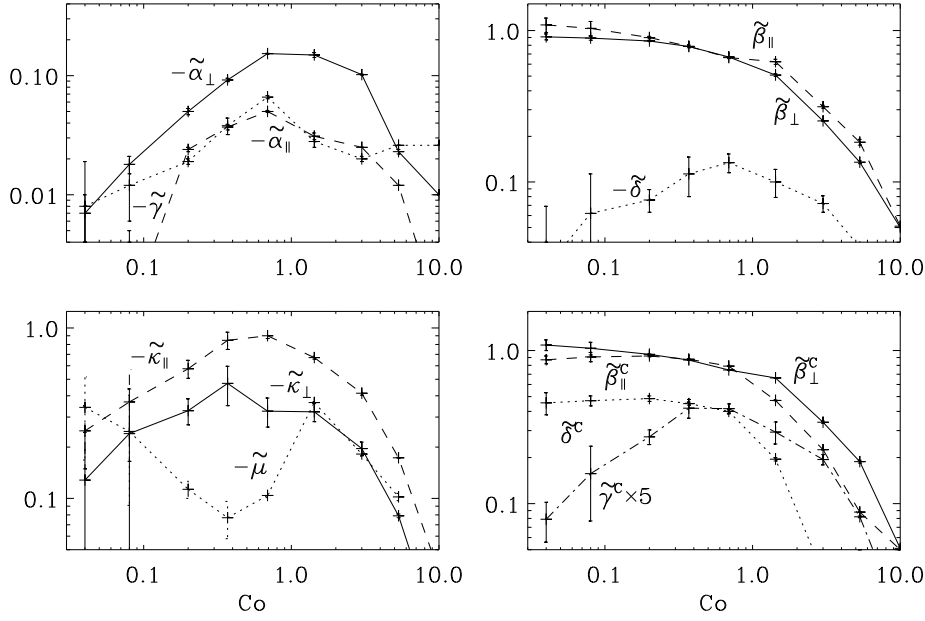


Fig. 18 Dependence of transport coefficients in a model with rotation and density stratification as a function of the Coriolis number, $Co = 2\Omega/u_{\text{rms}}k_f$. The other relevant parameters are $Re_M \approx 10$, $Gr = g/c_s^2 k_f \approx 0.16$, $k_f/k_1 = 5$, for $\nu = \eta = \kappa$.

with the stratification vector, although it can now attain a direction proportional to $\hat{\Omega}$ or the mean vorticity.

Owing to the presence of stratification and rotation, the turbulence attains helicity and can then produce an α effect. This has been studied in great detail in the past using analytic methods and, more recently, the test-field method. In Figure 18 we show an example from Brandenburg et al. (2012b), where the turbulence is governed by only one preferred direction, and $\hat{\Omega}$ and \mathbf{g} are therefore assumed to be parallel. In that case, $\overline{\mathcal{E}}$ can be represented in the form

$$\begin{aligned} \overline{\mathcal{E}} = & -\alpha_{\perp} \overline{\mathbf{B}} - (\alpha_{\parallel} - \alpha_{\perp})(\hat{\mathbf{e}} \cdot \overline{\mathbf{B}})\hat{\mathbf{e}} - \gamma \hat{\mathbf{e}} \times \overline{\mathbf{B}} \\ & -\beta_{\perp} \mu_0 \overline{\mathbf{J}} - (\beta_{\parallel} - \beta_{\perp})(\hat{\mathbf{e}} \cdot \mu_0 \overline{\mathbf{J}})\hat{\mathbf{e}} - \delta \hat{\mathbf{e}} \times \mu_0 \overline{\mathbf{J}} \\ & -\kappa_{\perp} \overline{\mathbf{K}} - (\kappa_{\parallel} - \kappa_{\perp})(\hat{\mathbf{e}} \cdot \overline{\mathbf{K}})\hat{\mathbf{e}} - \mu \hat{\mathbf{e}} \times \overline{\mathbf{K}} \end{aligned} \quad (33)$$

with nine coefficients $\alpha_{\perp}, \alpha_{\parallel}, \dots, \mu$.

Clearly, because of stratification and rotation, the turbulence is no longer isotropic, so α will also no longer be isotropic. In the simplest case when both \mathbf{g} and Ω are parallel, α has components parallel and perpendicular to their direction. The α effect is of particular interest, because it can lead to large-scale magnetic field generation. Another effect that is known to lead to large-scale dynamo action is the Rädler or $\Omega \times \mathbf{J}$ effect (Rädler 1969). Unlike the α effect, it exists already with just rotation and no stratification. Its astrophysical relevance is however still to be demonstrated. Note also that in all practical situations there must still be an additional source of energy, because $\Omega \times \overline{\mathbf{J}}$ has no component along $\overline{\mathbf{J}}$ and does therefore not provide energy to the system.

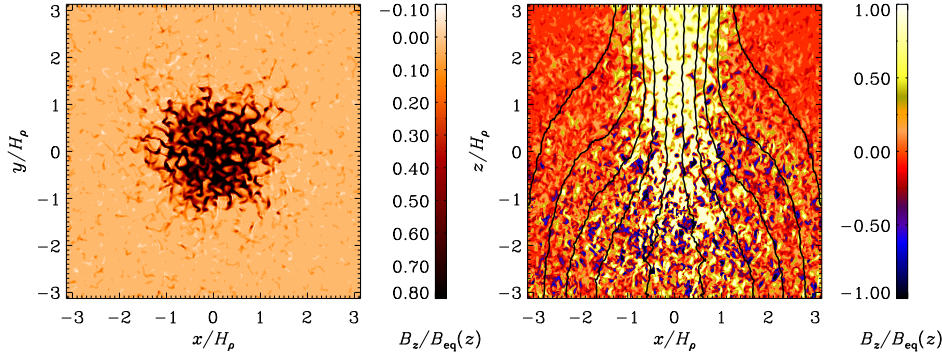


Fig. 19 Cuts of the vertical magnetic field in units of the equipartition field strength, $\overline{B}_z/B_{\text{eq}}(z)$, through the horizontal plane at the top boundary (left) and the vertical plane through the middle of the spot (right). Field lines of the numerically averaged mean field are superimposed. Adapted from Brandenburg et al. (2013).

6.4 Stratified turbulence with an imposed magnetic field

In the presence of an imposed magnetic field there is an important effect that deserves to be mentioned. In mean-field parameterizations of the Reynolds stress, there are terms that are quadratic in the mean magnetic field and contribute to a decrease of the Reynolds stress if there is a weak magnetic field. This suppression was discussed by Rüdiger (1974) and Rädler (1974) in connection with the understanding of the quenching of the α effect by a mean magnetic field. However, later it was understood that it also leads to a suppression of the turbulent pressure and that this suppression is stronger than the explicitly added magnetic pressure from the mean field, $\overline{B}^2/2\mu_0$. This means that the contribution of the mean field to the total turbulent pressure,

$$p_{\text{tot}} = p_{\text{gas}} + p_{\text{turb}} = p_{\text{gas}} + p_{\text{turb}}^{(0)} + [1 - q_p(\overline{B}^2/B_{\text{eq}}^2)] \overline{B}^2/2\mu_0, \quad (34)$$

which is embodied by the last term, $[1 - q_p(\overline{B}^2/B_{\text{eq}}^2)] \overline{B}^2/2\mu_0$, can be negative (Kleeorin et al. 1989, 1990, 1993, 1996; Kleeorin and Rogachevskii 1994; Rogachevskii and Kleeorin 2007). Here, $q_p(\overline{B}^2/B_{\text{eq}}^2)$ is a non-dimensional quenching function describing the suppression of the total stress, which consists of Reynolds and Maxwell stress. It is only a function of $\overline{B}^2/B_{\text{eq}}^2$, so even for a uniform \overline{B}^2 it can show spatial variation if B_{eq}^2 changes, for example as a result of density stratification. This allows the full dependence of q_p on $\overline{B}^2/B_{\text{eq}}^2$ to be probed in a single simulation (Brandenburg et al. 2012a; Kemel et al. 2012). The effect of the Maxwell stress turns out to be weaker than that of the Reynolds stress and it has the opposite effect, as was demonstrated by numerical calculations (Brandenburg et al. 2010).

In a stratified layer with a sub-equipartition magnetic fields this negative effective magnetic pressure can lead to an instability producing spontaneously magnetic flux concentrations (Kleeorin et al. 1989, 1993; Rogachevskii and Kleeorin 2007). This has recently been confirmed with DNS (Brandenburg et al. 2011; Kemel et al. 2012) and is being discussed in connection with explaining the spontaneous formation of active regions (Kemel et al. 2013) and sunspots (Brandenburg et al. 2013). In Figure 19 we show horizontal and vertical cuts through a magnetic spot from the simulation of Brandenburg et al. (2013) in the presence of an imposed vertical field. In the horizontal cut, again, strong fields correspond to dark

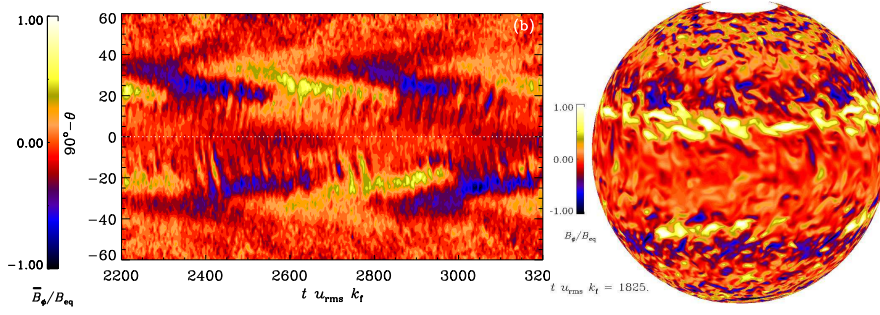


Fig. 20 *Left*: azimuthally averaged toroidal magnetic field as a function of time (in turnover times) and latitude (clipped between $\pm 60^\circ$). Note that on both sides of the equator ($90^\circ - \theta = \pm 25^\circ$), positive (yellow) and negative (blue) magnetic fields move equatorward, but the northern and southern hemispheres are slightly phase shifted relative to each other. *Right*: Snapshot of the toroidal magnetic field B_ϕ at $r = 0.98$ outer radii. Courtesy of Käpylä et al. (2012).

shades. The vertical cut is with a different color table where strong fields now correspond to light shades. It shows that the magnetic field (in units of the local equipartition field strength) decreases with height. Note also that the mean magnetic field fans out toward the bottom of the domain. Applying this finding to the origin of sunspots, it suggest that, contrary to common belief (cf. Brandenburg 2005), those structures may not be deeply anchored.

6.5 Solar dynamo and magnetic helicity fluxes

One of the main applications of mean-field theory has always been to explain the Sun's global magnetic field, its 11 year cycle, and the migration of magnetic field from mid to low latitudes, in addition, of course, eventually the formation of sunspots themselves. In the last few years, several groups have engaged in tackling the problem of the Sun's global magnetic field by performing numerical simulations of rotating turbulent convection in spherical shells using either spherical harmonics (Miesch and Toomre 2009; Brown et al. 2010, 2011), an implicit solver (Ghizaru et al. 2010; Racine et al. 2011), or finite differences in spherical wedges (Käpylä et al. 2010, 2012) to overcome the timestep constraint at the poles. The results from all groups trying to model the Sun agree in that they show equipartition-strength magnetic fields in the bulk of the convection zone (rather than highly super-equipartition-strength magnetic fields just at the bottom of the convection zone), with magnetic activity concentrated toward low latitudes and, in some cases, cyclic reversals of the magnetic field direction, resembling the solar 22 year cycle.

A major breakthrough has been achieved through the recent finding of equatorward migration of magnetic activity belts in the course of the cycle (Käpylä et al. 2012); see Figure 20. These results are robust and have now been reproduced in extended simulations that include a simplified model of an outer corona (Warnecke et al. 2013). Interestingly, the convection simulations of all three groups produce cycles only at rotation speeds that exceed those of the present Sun by a factor of 3–5 (Brown et al. 2011). Both lower and higher rotation speeds give, for example, different directions of the dynamo wave (Käpylä et al. 2012). Different rotation speeds correspond to different stellar ages (from 0.5 to 8 gigayears for rotation periods from 10 to 40 days), because magnetically active stars all have a wind and are subject to magnetic braking (Skumanich 1972). In addition, all simulations are subject

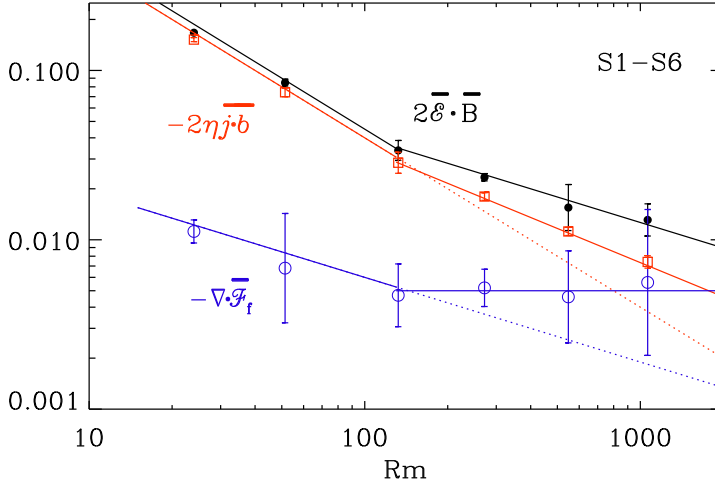


Fig. 21 Scaling properties of the vertical slopes of $2\overline{\mathcal{E}} \cdot \overline{\mathbf{B}}$, $-2\eta\mu_0 \overline{\mathbf{j}} \cdot \overline{\mathbf{b}}$, and $-\nabla \cdot \overline{\mathbf{F}}_f$. The three quantities vary approximately linearly with z , so the three labels indicate their non-dimensional values at $k_1 z = 1$. The dotted lines show the extrapolated initial scaling for low Re_M . Adapted from Del Sordo et al. (2013).

to systematic “errors” in that they poorly represent the small scales and emulate in that way an effective turbulent viscosity and magnetic diffusivity that is larger than in reality; see the corresponding discussion in Sect. 4.3.2 of Brandenburg et al. (2012a) in another context. In future simulations, it will therefore be essential to explore the range of possibilities by including stellar age as an additional dimension of the parameter space.

In support of our statement that a poor representation of the small scales in DNS emulates artificially enhanced turbulent viscosity and turbulent magnetic diffusivity, let us recall that η_t and α are scale-dependent. As discussed before in Section 5.5, they decrease with increasing k in a Lorentzian fashion. The relative importance of Ω effect over the α effect depends on the ratio of C_Ω and a similar parameter $C_\alpha = \alpha/\eta_t k$ characterizing the strength of the α effect. Both C_Ω and the ratio C_Ω/C_α would be underestimated in a large eddy simulation in which $\eta_t(k)k$ and $\alpha(k)$ are too big, so one would need to compensate for this shortcoming by increasing Ω to recover cyclic dynamo action.

As alluded to in Section 5.4, magnetic helicity fluxes play a major role in the dynamo by alleviating the otherwise catastrophic quenching of the dynamo (Blackman and Brandenburg 2003). Recent work using a simple model with a galactic wind has shown, for the first time, that this may indeed be possible. We recall that the evolution equation for the mean magnetic helicity density of fluctuating magnetic fields, $\overline{h}_f = \overline{\mathbf{a} \cdot \mathbf{b}}$, is

$$\frac{\partial \overline{h}_f}{\partial t} = -2\overline{\mathcal{E}} \cdot \overline{\mathbf{B}} - 2\eta\mu_0 \overline{\mathbf{j}} \cdot \overline{\mathbf{b}} - \nabla \cdot \overline{\mathbf{F}}_f, \quad (35)$$

where we allow two contributions to the flux of magnetic helicity from the fluctuating field $\overline{\mathbf{F}}_f$: an advective flux due to the wind, $\overline{\mathbf{F}}_f^w = \overline{h}_f \overline{\mathbf{U}}_w$, and a turbulent-diffusive flux due to turbulence, modelled by a Fickian diffusion term down the gradient of \overline{h}_f , i.e., $\overline{\mathbf{F}}_f^{\text{diff}} = -\kappa_h \nabla \overline{h}_f$. Here, $\overline{\mathcal{E}} = \overline{\mathbf{u} \times \mathbf{b}}$ is the electromotive force of the fluctuating field. The scaling of the terms on the right-hand side with Re_M has been considered before by Mitra et al. (2010) and Hubbard and Brandenburg (2010). They also drew attention to the fact that, even though

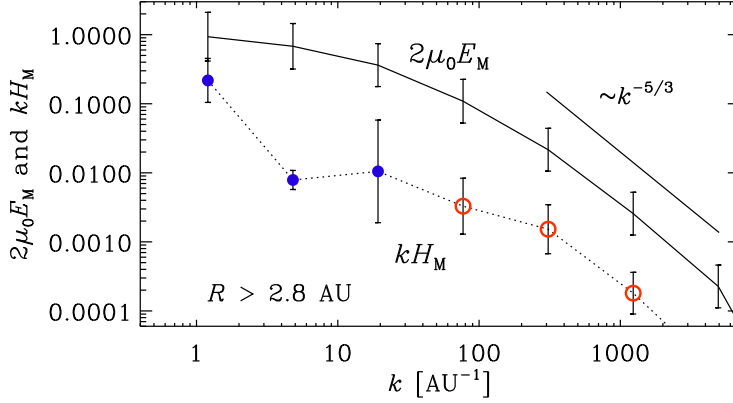


Fig. 22 Magnetic energy and helicity spectra, $2\mu_0 E_M(k)$ and $kH_M(k)$, respectively, for two separate distance intervals. Furthermore, both spectra are scaled by $4\pi R^2$ before averaging within each distance interval above 2.8 AU. Filled and open symbols denote negative and positive values of $H_M(k)$, respectively. Adapted from Brandenburg et al. (2011).

$\overline{\mathcal{F}_f}$ is gauge-invariant, the time average of $\nabla \cdot \overline{\mathcal{F}_f}$ is not, *provided* the system is statistically stationary and $\partial \overline{h_f} / \partial t$ vanishes on average.

In Figure 21 we show the basic result of Del Sordo et al. (2013). As it turns out, below $\text{Re}_M = 100$, the $2\eta\mu_0 \overline{\mathbf{j} \cdot \mathbf{b}}$ term dominates over $\nabla \cdot \overline{\mathcal{F}_f}$, but because of the different scalings (slopes being -1 and $-1/2$, respectively), the $\nabla \cdot \overline{\mathcal{F}_f}$ term is expected to become dominant for larger values of Re_M (about 3000). Unexpectedly, however, $\nabla \cdot \overline{\mathcal{F}_f}$ becomes approximately constant already for $\text{Re}_M \gtrsim 100$ and $2\eta\mu_0 \overline{\mathbf{j} \cdot \mathbf{b}}$ shows now a shallower scaling (slope $-1/2$). This means that the two curves would still cross at a similar value. Our data suggest, however, that $\nabla \cdot \overline{\mathcal{F}_f}$ may even rise slightly, so the crossing point is now closer to $\text{Re}_M = 1000$.

7 Solar wind observations

Solar wind observations provide a good way of determining the energy spectrum of MHD turbulence. As already mentioned in Section 5.2, recent work by Boldyrev et al. (2011) provides an explanation of why the kinetic and magnetic energy spectra have slightly different spectral indices in that the magnetic energy spectrum is slightly steeper ($\propto k^{-1.6}$) than that of the kinetic energy ($\propto k^{-1.4}$). This was found previously by Podesta et al. (2007). Indeed, looking again at Figure 8, it is clear that different slopes of kinetic and magnetic energy spectra is a consequence of the super-equipartition just below $k = k_f$ and the subsequent trend toward equipartition for larger values of k .

Solar wind observations have long been able to provide estimates about the magnetic helicity spectrum (Matthaeus et al. 1982). We recall that, even though the magnetic helicity is gauge-dependent, its spectrum is not. Technically, this is because the computation of the spectrum involves an integration over all space. In practice, this is not possible, of course. However, by making use of statistical homogeneity and the Taylor hypothesis of the equivalence of spatial and temporal Fourier spectra, Matthaeus et al. (1982) were able to express

the magnetic helicity spectrum as

$$H(k_R) = 4 \operatorname{Im}(\hat{B}_T \hat{B}_N^*) / k_R, \quad (36)$$

where $\hat{B}_T(k_R)$ and $\hat{B}_N(k_R)$ are the Fourier transforms of the two magnetic field components perpendicular to the radial direction away from the Sun, and (R, T, N) refers to the components of a locally Cartesian heliospheric coordinate system. Here, k_R is the wavenumber, which is related to the temporal frequency via $\omega = u_R k_R$, where $u_R \approx 800 \text{ km s}^{-1}$ is the wind speed at high heliographic latitudes. Note that in Equation (36), the expression for $H(k_R)$ is manifestly gauge-invariant.

Most spacecrafts have probed low heliographic latitudes, where the helicity is governed by fluctuations around zero. In recent years, however, it has been possible to estimate the magnetic helicity spectrum also at high heliographic latitudes using data from the Ulysses spacecraft that flew in a near-polar orbit. However, even at high heliographic latitudes the magnetic helicity is still strongly fluctuating and a clear sign of magnetic helicity can only be seen by averaging the spectra over broad, logarithmically spaced wavenumber bins; see Figure 22. One can define the *relative* spectral magnetic helicity, $2\mu_0 E_M(k)/k H_M(k)$, which is a non-dimensional quantity between -1 and 1 . It turns out that it is just a few percent. Nevertheless, the magnetic helicity is negative at large scales (small wavenumbers, $k < 30 \text{ AU}^{-1}$ corresponding to frequencies below 0.03 mHz) and positive at smaller scales (large wavenumbers); see Brandenburg et al. (2011). This agrees, at least qualitatively, with earlier results by Smith and Bieber (1993) that at low frequencies the magnetic helicity is negative in the northern hemisphere. At much higher frequencies (beyond 100 mHz), positive magnetic helicity in the northern hemisphere has now also been found by Podesta and Gary (2011).

When comparing with numerical simulations, it should be noted that virtually all observed spectra are based on one-dimensional measurements, while those of numerical simulations are based on the full three-dimensional velocity field. The two are related to each other via

$$E_M^{1D}(k_R) = \int_{k_R}^{\infty} E_M^{3D}(k) \, d \ln k, \quad (37)$$

$$H_M^{1D}(k_R) = \int_{k_R}^{\infty} H_M^{3D}(k) \, d \ln k. \quad (38)$$

This transformation is well known for the energy spectrum (cf., Tennekes and Lumley 1972; Dobler et al. 2003), and was recently generalized to the case with helicity (Brandenburg et al. 2011). The resulting one- and three-dimensional spectra agree in the case of pure power laws, but near the dissipative cutoff wavenumbers there is a sharp departure from power law behavior. This is significant in view of the fact that energy spectra of three-dimensional simulations indicate the presence of a so-called bottleneck effect (Falkovich 1994). This corresponds to an uprise of the compensated energy spectrum, $k^{5/3} E_K(k)$, near the dissipative cutoff wavenumber $k_\nu = \langle w^2 / \nu^2 \rangle^{1/4}$. This bottleneck effect is much weaker or absent in one-dimensional spectra (Dobler et al. 2003; Beresnyak and Lazarian 2009). The bottleneck might therefore be a real effect. Although it happens at such small scales that it should not be astrophysically significant, it does play a role in three-dimensional simulations and can lead to effects whose astrophysical significance needs to be assessed carefully in view of the fact that the growth rate of small-scale dynamos depends on the shape of the spectrum at the resistive scale; see Section 5.3.

8 Concluding comments

The last decades have been marked by important advances in our understanding of MHD turbulence. To a substantial degree this happened as numerical simulations became capable of producing high resolution MHD cubes. Therefore, MHD turbulence became a theory that can be tested. As a result of both analytical and numerical studies, as well as observational measurements of turbulence, the GS95 model of MHD turbulence has been established as the most promising model. While we believe that the model is not complete in detail (e.g. in terms of intermittency), it is able to describe the astrophysically important properties of turbulence, for instance, the scale dependence of local anisotropy important for cosmic ray propagation, and the magnetic field wandering important for heat transfer and magnetic reconnection.

The physical ideas of the GS95 model have been extended and applied to successfully describing compressible MHD turbulence. It has been shown that the low coupling of fast and Alfvén modes allows the independent treatment of the Alfvénic cascade, which is very important; see Section 3.2. Indeed, it allows one to use the GS95 scaling for describing Alfvénic modes in moderately compressible fluids, which is of major astrophysical significance.

However, there are many issues that require further studies. Those include the properties of highly compressible, highly supersonic MHD turbulence, scaling and properties of fast modes etc. Last but not the least, more work is required for the highly debated subject of imbalanced turbulence. The corresponding studies call for extensive numerical efforts to test the existing theories. We hope that many of these currently controversial issues will be solved in the near future. This has important applications for turbulent dynamos of all sorts. It is now clear that nonlinear turbulent dynamos work also at small magnetic Prandtl numbers, even though the excitation conditions for kinematic dynamos become prohibitively high at low magnetic Prandtl numbers of around 0.1. As discussed in Section 5.3, the reason for this has meanwhile been identified as the bottleneck effect in turbulence.

Large-scale dynamos are affected by similar subtleties. They are in particular subject to the possibility of catastrophic quenching, which means that dynamos and their underlying turbulent transport coefficients remain dependent on the magnetic Reynolds numbers. Astrophysical dynamos are believed to be independent of Re_M , but we now know that most dynamos in DNS are probably not yet in that regime, but there is not much doubt that such a regime exists that is independent of the magnetic Reynolds number. In practice, this is accomplished by magnetic helicity fluxes. Regarding solar and stellar dynamo theory, the reason for equatorward migration of magnetic activity belts is still not understood. This is an example where simulations might now lead the way toward explaining the observed solar behavior, but more progress is needed to fully understand the physics behind the behavior seen in simulations.

Acknowledgements We thank Andre Balogh for providing an inspiring atmosphere at the International Space Science Institute in Bern in 2012, which has led to new collaborations and scientific progress. Computing resources were provided by the Swedish National Allocations Committee at the Center for Parallel Computers at the Royal Institute of Technology in Stockholm and the High Performance Computing Center North in Umeå. This work was supported in part by the European Research Council under the AstroDyn Research Project No. 227952 and the Swedish Research Council under the project grants 621-2011-5076 and 2012-5797. AL acknowledges the support of the NSF grant AST-1212096, the NASA grant NNX09AH78G, the Vilas Associate Award as well as the support of the NSF Center for Magnetic Self-Organization. In addition, AL thanks the International Institute of Physics (Natal, Brazil) for its hospitality during the work on this review.

References

- J. W. Armstrong, B. J. Rickett, S. R. Spangler, Electron density power spectrum in the local interstellar medium, *Astrophys. J.* **443**, 209-221 (1995)
- R. Banerjee, K. Jedamzik, Evolution of cosmic magnetic fields: From the very early Universe, to recombination, to the present, *Phys. Rev. D* **70**, 123003 (2004)
- S. Banerjee, S. Galtier, Exact relation with two-point correlation functions and phenomenological approach for compressible magnetohydrodynamic turbulence, *Phys. Rev. E* **87**, 013019 (2013)
- G.K. Batchelor, On the spontaneous magnetic field in a conducting liquid in turbulent motion, *Proc. Roy. Soc. Lond.* **A201**, 405-416 (1950)
- R. Beck, A. Brandenburg, D. Moss, A. Shukurov, D. Sokoloff, Galactic magnetism: recent developments and perspectives, *Ann. Rev. Astron. Astrophys.* **34**, 155-206 (1996)
- A.R. Bell, Turbulent amplification of magnetic field and diffusive shock acceleration of cosmic rays, *Monthly Notices Roy. Astron. Soc.* **353**, 550-558 (2004)
- A. Beresnyak, Spectral slope and Kolmogorov constant of MHD turbulence, *Phys. Rev. Lett.* **106**, 075001 (2011)
- A. Beresnyak, Basic properties of magnetohydrodynamic turbulence in the inertial range, *Monthly Notices Roy. Astron. Soc.* **422**, 3495-3502 (2012)
- A. Beresnyak, T.W. Jones, A. Lazarian, Turbulence-induced magnetic fields and structure of cosmic ray modified shocks, *Astrophys. J.* **707**, 1541-1549 (2009)
- A. Beresnyak, A. Lazarian, Strong imbalanced turbulence, *Astrophys. J. Lett.* **682**, 1070-1075 (2008)
- A. Beresnyak, A. Lazarian, Comparison of spectral slopes of magnetohydrodynamic and hydrodynamic turbulence and measurements of alignment effects, *Astrophys. J. Lett.* **702**, 1190-1198 (2009)
- A. Beresnyak, A. Lazarian, Scaling laws and diffuse locality of balanced and imbalanced magnetohydrodynamic turbulence, *Astrophys. J. Lett.* **722**, L110-L113 (2010)
- A. Beresnyak, A. Lazarian, J. Cho, Density scaling and anisotropy in supersonic magnetohydrodynamic turbulence, *Astrophys. J. Lett.* **624**, L93-L96 (2005)
- P. Bhat and K. Subramanian, Fluctuation dynamos and their Faraday rotation signatures, *Monthly Notices Roy. Astron. Soc.* **429**, 2469-2481 (2013)
- D. Biskamp and W.-C. Müller, Decay laws for three-dimensional magnetohydrodynamic turbulence, *Phys. Rev. Lett.* **83**, 2195-2198 (1999)
- D. Biskamp, *Magnetohydrodynamic Turbulence*. Cambridge: Cambridge University Press (2003)
- E.G. Blackman and A. Brandenburg, Doubly helical coronal ejections from dynamos and their role in sustaining the solar cycle, *Astrophys. J. Lett.* **584**, L99-L102 (2003)
- E.G. Blackman, G.B. Field, Dimensionless measures of turbulent magnetohydrodynamic dissipation rates, *Monthly Notices Roy. Astron. Soc.* **386**, 1481-1486 (2008)
- S. Boldyrev, On the spectrum of magnetohydrodynamic turbulence, *Astrophys. J. Lett.* **626**, L37-L40 (2005)
- S. Boldyrev, Spectrum of magnetohydrodynamic turbulence, *Phys. Rev. Lett.* **96**, 115002 (2006)
- S.A. Boldyrev, F. Cattaneo, Magnetic-field generation in Kolmogorov turbulence, *Phys. Rev. Lett.* **92**, 144501 (2004)
- S. Boldyrev, Å. Nordlund and P. Padoan, Scaling relations of supersonic turbulence in star-forming molecular clouds, *Astrophys. J.* **573**, 678-684 (2002)
- S. Boldyrev, J.C. Perez, J.E. Borovsky, J.J. Podesta, Spectral scaling laws in magnetohydrodynamic turbulence simulations and in the solar wind, *Astrophys. J.* **741**, L19 (2011)
- A. Brandenburg, The case for a distributed solar dynamo shaped by near-surface shear, *Astrophys. J.* **625**, 539-547 (2005)
- A. Brandenburg, Nonlinear small-scale dynamos at low magnetic Prandtl numbers, *Astrophys. J.* **741**, 92 (2011)
- A. Brandenburg, Å. Nordlund, Astrophysical turbulence modeling, *Rep. Prog. Phys.* **74**, 046901 (2011)
- A. Brandenburg, K. Subramanian, Astrophysical magnetic fields and nonlinear dynamo theory, *Phys. Rep.* **417**, 1-209 (2005)
- A. Brandenburg, K. Enqvist, P. Olesen, Large-scale magnetic fields from hydromagnetic turbulence in the very early universe, *Phys. Rev. D* **54**, 1291-1300 (1996)
- A. Brandenburg, P. Käpylä, and A. Mohammed, A., Non-Fickian diffusion and tau-approximation from numerical turbulence, *Phys. Fluids* **16**, 1020-1027 (2004)
- A. Brandenburg, N. Kleeorin, I. Rogachevskii, Large-scale magnetic flux concentrations from turbulent stresses, *Astron. Nachr.* **331**, 5-13 (2010)
- A. Brandenburg, N. Kleeorin, I. Rogachevskii, Self-assembly of shallow magnetic spots through strongly stratified turbulence, *Astrophys. J. Lett.*, submitted, arXiv:1306.4915 (2013)

- A. Brandenburg, K.-H. Rädler, M. Rheinhardt, and K. Subramanian, Magnetic quenching of alpha and diffusivity tensors in helical turbulence, *Astrophys. J.* **676**, 740-L52 (2008a)
- A. Brandenburg, K.-H. Rädler, M. Schrunner, Scale dependence of alpha effect and turbulent diffusivity, *Astron. Astrophys.* **482**, 739-746 (2008b)
- A. Brandenburg, K. Subramanian, A. Balogh, M.L. Goldstein, Scale-dependence of magnetic helicity in the solar wind, *Astrophys. J.* **734**, 9 (2011)
- A. Brandenburg, K. Kemel, N. Kleeorin, D. Mitra, I. Rogachevskii, Detection of negative effective magnetic pressure instability in turbulence simulations, *Astrophys. J.* **740**, L50 (2011)
- A. Brandenburg, K. Kemel, N. Kleeorin, I. Rogachevskii, The negative effective magnetic pressure in stratified forced turbulence, *Astrophys. J.* **749**, 179 (2012a)
- A. Brandenburg, K.-H. Rädler, K. Kemel, Mean-field transport in stratified and/or rotating turbulence, *Astron. Astrophys.* **539**, A35 (2012b)
- A. Brandenburg, D. Sokoloff, K. Subramanian, Current status of turbulent dynamo theory: From large-scale to small-scale dynamos, *Spa. Sci. Rev.* **169**, 123-157 (2012c)
- B.P. Brown, M.K. Browning, A.S. Brun, M.S. Miesch, J. Toomre, Persistent magnetic wreaths in a rapidly rotating Sun, *Astrophys. J.* **711**, 424-438 (2010)
- B.P. Brown, M.S. Miesch, M.K. Browning, A.S. Brun, J. Toomre, Magnetic cycles in a convective dynamo simulation of a young solar-type star, *Astrophys. J.* **731**, 69 (2011)
- G. Brunetti, A. Lazarian, Compressible turbulence in galaxy clusters: physics and stochastic particle re-acceleration, *Monthly Notices Roy. Astron. Soc.* **378**, 245-275 (2007)
- B. Burkhart, A. Lazarian, V. Ossenkopf, J. Stutzki, The turbulence power spectrum in optically thick interstellar clouds, *Astrophys. J.* **771**, 123 (2013)
- A.M. Bykov, A. Brandenburg, M.A. Malkov, S.M. Osipov, Microphysics of cosmic ray driven plasma instabilities, *Spa. Sci. Rev.*, DOI: 10.1007/s11214-013-9988-3 (2013)
- S. Candelaresi, A. Brandenburg, How much helicity is needed to drive large-scale dynamos? *Phys. Rev. E* **87**, 043104 (2013)
- B.D.G. Chandran, S.C. Cowley, Thermal conduction in a tangled magnetic field, *Phys. Rev. Lett.* **80**, 3077-3080 (1998)
- B.D.G. Chandran, Scattering of energetic particles by anisotropic magnetohydrodynamic turbulence with a Goldreich-Sridhar power spectrum, *Phys. Rev. Lett.* **85**, 4656-4659 (2000)
- L. Chamandy, K. Subramanian, A. Shukurov, Galactic spiral patterns and dynamo action - I. A new twist on magnetic arms, *Monthly Notices Roy. Astron. Soc.* **428**, 3569-3589 (2013)
- P. Chatterjee, G. Guerrero, A. Brandenburg, Magnetic helicity fluxes in interface and flux transport dynamos, *Astron. Astrophys.* **525**, A5 (2011)
- A. Chepurnov, A. Lazarian, Turbulence spectra from Doppler-broadened spectral lines: tests of the velocity channel analysis and velocity coordinate spectrum techniques, *Astrophys. J.* **693**, 1074-1083 (2009)
- A. Chepurnov, A. Lazarian, Extending the Big Power Law in the Sky with turbulence spectra from Wisconsin H α Mapper Data, *Astrophys. J.* **710**, 853-858 (2010)
- J. Cho, A. Lazarian, Compressible sub-Alfvénic MHD turbulence in low- β plasmas, *Phys. Rev. Lett.* **88**, 245001 (2002) (CL02)
- J. Cho, A. Lazarian, Compressible magnetohydrodynamic turbulence: mode coupling, scaling relations, anisotropy, viscosity-damped regime and astrophysical implications, *Monthly Notices Roy. Astron. Soc.* **345**, 325-339 (2003) (CL03)
- J. Cho, A. Lazarian, Thermal conduction in magnetized turbulent gas, *J. Korean Astron. Soc.* **37**, 557-562 (2004)
- J. Cho and A. Lazarian, Grain alignment by radiation in dark clouds and cores, *Astrophys. J.* **631**, 361-370 (2005)
- J. Cho, A. Lazarian, E.T. Vishniac, Simulations of magnetohydrodynamic turbulence in a strongly magnetized medium, *Astrophys. J.* **564**, 291-301 (2002)
- J. Cho and E.T. Vishniac, The generation of magnetic fields through driven turbulence, *Astrophys. J.* **538**, 217-225 (2000)
- J. Crovisier, J.M. Dickey, The spatial power spectrum of galactic neutral hydrogen from observations of the 21-cm emission line, *Astron. Astrophys.* **122**, 282-296 (1983)
- R.M. Crutcher, B. Wandelt, C. Heiles, E. Falgarone, T.H. Troland, Magnetic fields in interstellar clouds from Zeeman observations: inference of total field strengths by Bayesian analysis, *Astrophys. J.* **725**, 466-479 (2010)
- F. Del Sordo, G. Guerrero, A. Brandenburg, Turbulent dynamo with advective magnetic helicity flux, *Monthly Notices Roy. Astron. Soc.* **429**, 1686-1694 (2013)
- R.L. Dickman, S.C. Kleiner, Large-scale structure of the Taurus molecular complex – Part three – Methods for turbulence, *Astrophys. J.* **295**, 479-484 (1985)

- W. Dobler, N. E. L. Haugen, T. A. Yousef, A. Brandenburg, Bottleneck effect in three-dimensional turbulence simulations, *Phys. Rev. E* **68**, 026304 (2003)
- T.A. Enßlin, C. Vogt, Magnetic turbulence in cool cores of galaxy clusters, *Astron. Astrophys.* **453**, 447-458 (2006)
- A. Esquivel, A. Lazarian, S. Horibe, J. Cho, V. Ossenkopf, J. Stutzki, Statistics of velocity centroids: effects of density-velocity correlations and non-Gaussianity, *Monthly Notices Roy. Astron. Soc.* **381**, 1733-1744 (2007)
- G.L. Eyink, A. Lazarian, E.T. Vishniac, Fast magnetic reconnection and spontaneous stochasticity, *Astrophys. J.* **743**, 51 (2011)
- B.G. Elmegreen, J. Scalo, Interstellar turbulence I: observations and processes, *Ann. Rev. Astron. Astrophys.* **42**, 211-273 (2004)
- G. Falkovich, Bottleneck phenomenon in developed turbulence, *Phys. Fluids* **6**, 1411-1414 (1994)
- S. Galtier, S. Banerjee, Exact Relation for Correlation Functions in Compressible Isothermal Turbulence, *Phys. Rev. Lett.* **107**, 134501 (2011)
- S. Galtier, S.V. Nazarenko, A.C. Newell, A. Pouquet, A weak turbulence theory for incompressible magneto-hydrodynamics, *J. Plasm. Phys.* **63**, 447-488 (2000)
- M. Ghizaru, P. Charbonneau, P.K. Smolarkiewicz, Magnetic cycles in global large-eddy simulations of solar convection, *Astrophys. J.* **715**, L133-L137 (2010)
- P.A. Gilman, Dynamically consistent nonlinear dynamos driven by convection in a rotating spherical shell. II. Dynamos with cycles and strong feedbacks, *Astrophys. J. Suppl.* **53**, 243-268 (1983)
- P. Goldreich and S. Sridhar, Toward a theory of interstellar turbulence. 2. Strong Alfvénic turbulence, *Astrophys. J.* **438**, 763-775 (1995) (GS95)
- P. Goldreich and S. Sridhar, Magnetohydrodynamic turbulence revisited, *Astrophys. J.* **485**, 680-688 (1997)
- G.A. Glatzmaier, Numerical simulations of stellar convective dynamos. II. Field propagation in the convection zone, *Astrophys. J.* **291**, 300-307 (1985)
- J. Goodman, R. Narayan, Slow pulsar scintillation and the spectrum of interstellar electron density fluctuations, *Monthly Notices Roy. Astron. Soc.* **214**, 519-537 (1985)
- D.A. Green, A power spectrum analysis of the angular scale of Galactic neutral hydrogen emission towards $L = 140^\circ$, $B = 0^\circ$, *Monthly Notices Roy. Astron. Soc.* **262**, 327-342 (1993)
- A. Gruzinov, S. Cowley, R. Sudan, Small-scale-field dynamo, *Phys. Rev. Lett.* **77**, 4342-4345 (1996)
- N.E.L. Haugen, A. Brandenburg, W. Dobler, Is nonhelical hydromagnetic turbulence peaked at small scales?, *Astrophys. J.* **597**, L141-L144 (2003)
- N.E.L. Haugen, A. Brandenburg, W. Dobler, Simulations of nonhelical hydromagnetic turbulence, *Phys. Rev. E* **70**, 016308 (2004a)
- N.E.L. Haugen, A. Brandenburg, A.J. Mee, Mach number dependence of the onset of dynamo action, *Monthly Notices Roy. Astron. Soc.* **353**, 947-952 (2004b)
- N.E.L. Haugen, A. Brandenburg, Hydrodynamic and hydromagnetic energy spectra from large eddy simulations, *Phys. Fluids* **18**, 075106 (2006)
- J.C. Higdon, Density fluctuations in the interstellar medium. Evidence for anisotropic magnetogas turbulence. I. Model and astrophysical sites, *Astrophys. J.* **285**, 109-123 (1984)
- A. Hubbard, A. Brandenburg, Memory effects in turbulent transport, *Astrophys. J.* **706**, 712-726 (2009)
- A. Hubbard, A. Brandenburg, Magnetic helicity fluxes in an α^2 dynamo embedded in a halo, *Geophys. Astrophys. Fluid Dynam.* **104**, 577-590 (2010)
- R.S. Iroshnikov, Turbulence of a conducting fluid in a strong magnetic field, *Sov. Astron.* **7**, 566-571 (1963)
- A.B. Isakov, A.A. Schekochihin, S.C. Cowley, J.C. McWilliams, M.R.E. Proctor, Numerical demonstration of fluctuation dynamo at low magnetic Prandtl numbers, *Phys. Rev. Lett.* **98**, 208501 (2007)
- J.R. Jokipii, Pitch-angle scattering of charged particles in a random magnetic field, *Astrophys. J.* **194**, 465-469 (1974)
- T. Kahniashvili, A. Brandenburg, A.G. Tevzadze, B. Ratra, Numerical simulations of the decay of primordial magnetic turbulence, *Phys. Rev. D* **81**, 123002 (2010)
- T. Kahniashvili, A.G. Tevzadze, A. Brandenburg, A. Neronov, Evolution of primordial magnetic fields from phase transitions, *Phys. Rev. D* **87**, 083007 (2013)
- P.J. Käpylä, M.J. Korpi, A. Brandenburg, D. Mitra, R. Tavakol, Convective dynamos in spherical wedge geometry, *Astron. Nachr.* **331**, 73-81 (2010)
- P.J. Käpylä, M.J. Mantere, A. Brandenburg, Cyclic magnetic activity due to turbulent convection in spherical wedge geometry, *Astrophys. J. Lett.* **755**, L22 (2012)
- P.J. Käpylä, A. Brandenburg, N. Kleeorin, M.J. Mantere, I. Rogachevskii, Negative effective magnetic pressure in turbulent convection, *Monthly Notices Roy. Astron. Soc.* **422**, 2465-2473 (2012)
- A.P. Kazantsev, Enhancement of a magnetic field by a conducting fluid, *Sov. Phys. JETP* **26**, 1031-1034 (1968)

- K. Kemel, A. Brandenburg, N. Kleeorin, D. Mitra, I. Rogachevskii, Spontaneous formation of magnetic flux concentrations in stratified turbulence, *Solar Phys.* **280**, 321-333 (2012)
- K. Kemel, A. Brandenburg, N. Kleeorin, D. Mitra, I. Rogachevskii, Active region formation through the negative effective magnetic pressure instability, *Solar Phys.*, DOI:10.1007/s11207-012-0031-8 (2013)
- S. Kida, S. Yanase, J. Mizushima, Statistical properties of MHD turbulence and turbulent dynamo, *Phys. Fluids A* **3**, 457-465 (1991)
- L.L. Kitchatinov, A. Brandenburg, Transport of angular momentum and chemical species by anisotropic mixing in stellar radiative interiors, *Astron. Nachr.* **333**, 230-236 (2012)
- N.I. Kleeorin, I.V. Rogachevskii, A.A. Ruzmaikin, Negative magnetic pressure as a trigger of large-scale magnetic instability in the solar convective zone, *Sov. Astron. Lett.* **15**, 274-277 (1989)
- N.I. Kleeorin, I.V. Rogachevskii, A.A. Ruzmaikin, Magnetic force reversal and instability in a plasma with advanced magnetohydrodynamic turbulence, *Sov. Phys. JETP* **70**, 878-883 (1990)
- N. Kleeorin, I. Rogachevskii, Effective Ampère force in developed magnetohydrodynamic turbulence, *Phys. Rev. E* **50**, 2716-2730 (1994)
- N. Kleeorin, M. Mond, I. Rogachevskii, Magnetohydrodynamic instabilities in developed small-scale turbulence, *Phys. Fluids* **5**, 4128-4134 (1993)
- N. Kleeorin, M. Mond, I. Rogachevskii, Magnetohydrodynamic turbulence in the solar convective zone as a source of oscillations and sunspots formation, *Astron. Astrophys.* **307**, 293-309 (1996)
- A.N. Kolmogorov, The local structure of turbulence in incompressible viscous fluid for very large Reynolds numbers, *CR Acad. Sci. USSR* **30**, 299-303 (1941)
- G. Kowal, A. Lazarian, A. Beresnyak, Density fluctuations in MHD turbulence: spectra, intermittency, and topology, *Astrophys. J.* **658**, 423-445 (2007)
- G. Kowal, A. Lazarian, Velocity field of compressible magnetohydrodynamic turbulence: wavelet decomposition and mode scalings, *Astrophys. J.* **720**, 742-756 (2010)
- R.H. Kraichnan, Inertial-range spectrum of hydromagnetic turbulence, *Phys. Fluids* **8**, 1385-1387 (1965)
- F. Krause, K.-H. Rädler, *Mean-field Magnetohydrodynamics and Dynamo Theory*. Oxford: Pergamon Press (1980)
- A.G. Kritsuk, M.L. Norman, P. Padoan, R. Wagner, The statistics of supersonic isothermal turbulence, *Astrophys. J.* **665**, 416-431 (2007)
- A.G. Kritsuk, Å. Nordlund, D. Collins, P. Padoan, M.L. Norman, T. Abel, R. Banerjee, C. Federrath, M. Flock, D. Lee, P.S. Li, W.-C. Müller, R. Teyssier, S. D. Ustyugov, C. Vogel, H. Xu, Comparing numerical methods for isothermal magnetized supersonic turbulence, *Astrophys. J.* **737**, 13 (2011)
- R.M. Kulsrud, A critical review of galactic dynamos, *Ann. Rev. Astron. Astrophys.* **37**, 37-64 (1999)
- A. Lazarian, Astrophysical implications of turbulent reconnection: from cosmic rays to star formation, In *Magnetic fields in the Universe* (ed. E. de Gouveia Dal Pino, G. Lugones, A. Lazarian), pp. 42-54. AIP, vol. **784** (2005)
- A. Lazarian, Enhancement and Suppression of Heat Transfer by MHD Turbulence, *Astrophys. J. Lett.* **645**, L25-L28 (2006) (L06)
- A. Lazarian, Obtaining Spectra of Turbulent Velocity from Observations, *Spa. Sci. Rev.* **143**, 357-385 (2009)
- A. Lazarian, A. Esquivel, Statistics of velocity from spectral data: modified velocity centroids, *Astrophys. J.* **592**, L37-L40 (2003)
- A. Lazarian, A. Esquivel, Velocity centroids as tracers of the turbulent velocity statistics, *Astrophys. J.* **631**, 320-350 (2005)
- A. Lazarian, D. Pogosyan, Velocity modification of HI power spectrum, *Astrophys. J.* **537**, 720-748 (2000) (LP00)
- A. Lazarian, D. Pogosyan, Velocity modification of the power spectrum from an absorbing medium, *Astrophys. J.* **616**, 943-965 (2004)
- A. Lazarian, D. Pogosyan, Statistics of fluctuations along velocity coordinate: effects of absorption, *Astrophys. J.* **652**, 1348-1348 (2006)
- A. Lazarian, D. Pogosyan, Studying velocity turbulence from Doppler-broadened absorption lines: statistics of optical depth fluctuations, *Astrophys. J.* **686**, 350-362 (2008)
- A. Lazarian and E.T. Vishniac, Reconnection in a weakly stochastic field, *Astrophys. J.* **517**, 700-718 (1999) (LV99)
- A. Lazarian and E.T. Vishniac, Model of reconnection of weakly stochastic magnetic field and its implications, *Rev. Mex. Astron. Astrof. Conf. Ser.* **36**, 81-88 (2009)
- A. Lazarian, A. Esquivel, R. Crutcher, Magnetization of cloud cores and envelopes and other observational consequences of reconnection diffusion, *Astrophys. J.* **757**, 154 (2012a)
- A. Lazarian, L. Vlahos, G. Kowal, H. Yan, A. Beresnyak, E.M. de Gouveia Dal Pino, Turbulence, magnetic reconnection in turbulent fluids and energetic particle acceleration, *Spa. Sci. Rev.* **173**, 557-622 (2012b)
- M. Lesieur, *Turbulence in Fluids*. Martinus Nijhoff Publishers, Dordrecht (1990)

- Y. Lithwick, P. Goldreich, P., Imbalanced weak magnetohydrodynamic turbulence, *Astrophys. J.* **582**, 1220-1240 (2003)
- Y. Lithwick, P. Goldreich, S. Sridhar, Imbalanced strong MHD turbulence, *Astrophys. J.* **655**, 269-274 (2007)
- J. Maron and P. Goldreich, Simulations of incompressible magnetohydrodynamic turbulence, *Astrophys. J.* **554**, 1175-1196 (2001)
- W.H. Matthaeus, M.L. Goldstein, C. Smith, Evaluation of magnetic helicity in homogeneous turbulence, *Phys. Rev. Lett.* **48**, 1256-1259 (1982)
- D.B. Melrose, The emission and absorption of waves by charged particles in magnetized plasmas, *Astrophys. Spa. Sci.* **2**, 171-235 (1968)
- M. Meneguzzi, U. Frisch, A. Pouquet, Helical and nonhelical turbulent dynamos, *Phys. Rev. Lett.* **47**, 1060-1064 (1981)
- M. Meneguzzi, A. Pouquet, Turbulent dynamos driven by convection, *J. Fluid Mech.* **205**, 297-312 (1989)
- M.S. Miesch, J. Scalo, J. Bally, Velocity field statistics in star-forming regions. I. Centroid velocity observations, *Astrophys. J.* **524**, 895-922 (1999)
- M.S. Miesch, J. Toomre, Turbulence, magnetism, and shear in stellar interiors, *Ann. Rev. Fluid Dyn.* **41**, 317-345 (2009)
- D. Mitra, P. J. Käpylä, R. Tavakol, and A. Brandenburg, Alpha effect and diffusivity in helical turbulence with shear, *Astron. Astrophys.* **495**, 1-8 (2009)
- D. Mitra, S. Candelaresi, P. Chatterjee, R. Tavakol, A. Brandenburg, Equatorial magnetic helicity flux in simulations with different gauges, *Astron. Nachr.* **331**, 130-135 (2010)
- M.-A. Miville-Deschênes, G. Joncas, E. Falgarone, F. Boulanger, High resolution 21 cm mapping of the Ursa Major Galactic cirrus: Power spectra of the high-latitude H I gas, *Astron. Astrophys.* **411**, 109-121 (2003)
- H.K. Moffatt, *Magnetic Field Generation in Electrically Conducting Fluids*. Cambridge: Cambridge Univ. Press (1978)
- G. Münch, Internal motions in the Orion nebula, *Rev. Mod. Phys.* **30**, 1035-1041 (1958)
- R. Narayan, M.V. Medvedev, Thermal conduction in clusters of galaxies, *Astrophys. J.* **562**, L129-L132 (2001)
- C.S. Ng and A. Bhattacharjee, Interaction of shear-Alfvén wave packets: Implication for weak magnetohydrodynamic turbulence in astrophysical plasmas, *Astrophys. J.* **465**, 845-854 (1996)
- Å. Nordlund, A. Brandenburg, R.L. Jennings, M. Rieutord, J. Ruokolainen, R.F. Stein, I. Tuominen, Dynamo action in stratified convection with overshoot, *Astrophys. J.* **392**, 647-652 (1992)
- C.R. O'dell, H.O. Castaneda, Evidence for turbulence in H II regions, *Astrophys. J.* **317**, 686-692 (1987)
- P. Padoan, M. Juvela, A. Kritsuk, M.L. Norman, The power spectrum of supersonic turbulence in Perseus, *Astrophys. J. Lett.* **653**, 125-128 (2006)
- P. Padoan, M. Juvela, A. Kritsuk, M.L. Norman, The power spectrum of turbulence in NGC 1333: outflows or large-scale driving?, *Astrophys. J. Lett.* **707**, L153-L157 (2009)
- E.N. Parker, *Cosmical magnetic fields*. Clarendon Press, Oxford (1979)
- J.C. Perez, S. Boldyrev, Role of cross-helicity in magnetohydrodynamic turbulence, *Phys. Rev. Lett.* **102**, 025003 (2009)
- V. Petrosian, H. Yan, A. Lazarian, Damping of magnetohydrodynamic turbulence in solar flares, *Astrophys. J.* **644**, 603-612 (2006)
- V.V. Pipin, The mean electro-motive force and current helicity under the influence of rotation, magnetic field and shear, *Geophys. Astrophys. Fluid Dynam.* **102**, 21-49 (2008)
- J.J. Podesta, D.A. Roberts, M.L. Goldstein, Spectral exponents of kinetic and magnetic energy spectra in solar wind turbulence, *Astrophys. J.* **664**, 543-548 (2007)
- J.J. Podesta, S.P. Gary, Magnetic helicity spectrum of solar wind fluctuations as a function of the angle with respect to the local mean magnetic field, *Astrophys. J.* **734**, 15 (2011)
- K.-H. Rädler, On some electromagnetic phenomena in electrically conducting turbulently moving matter, especially in the presence of Coriolis forces, *Geod. Geophys. Veröff., Reihe II* **13**, 131-135 (1969)
- K.-H. Rädler, On the influence of a large-scale magnetic field on turbulent motions in an electrically conducting medium, *Astron. Nachr.* **295**, 265-273 (1974)
- É. Racine, P. Charbonneau, M. Ghizaru, A. Bouchat, P.K. Smolarkiewicz, On the mode of dynamo action in a global large-eddy simulation of solar convection, *Astrophys. J.* **735**, 46 (2011)
- K.-H. Rädler, A. Brandenburg, F. Del Sordo, M. Rheinhardt, Mean-field diffusivities in passive scalar and magnetic transport in irrotational flows, *Phys. Rev. E* **84**, 4 (2011)
- A.B. Rechester, M.N. Rosenbluth, Electron heat transport in a Tokamak with destroyed magnetic surfaces, *Phys. Rev. Lett.* **40**, 38-41 (1978)
- M. Rheinhardt and A. Brandenburg, Test-field method for mean-field coefficients with MHD background, *Astron. Astrophys.* **520**, A28 (2010)

- M. Rheinhardt, A. Brandenburg, Modeling spatio-temporal nonlocality in mean-field dynamos, *Astron. Nachr.* **333**, 71-77 (2012)
- I. Rogachevskii, N. Kleeorin, A. Brandenburg, D. Eichler, Cosmic ray current-driven turbulence and mean-field dynamo effect, *Astrophys. J.* **753**, 6 (2012)
- I. Rogachevskii, N. Kleeorin, Intermittency and anomalous scaling for magnetic fluctuations, *Phys. Rev. E* **56**, 417-426 (1997)
- I. Rogachevskii, N. Kleeorin, Magnetic fluctuations and formation of large-scale inhomogeneous magnetic structures in a turbulent convection, *Phys. Rev. E* **76**, 056307 (2007)
- G. Rüdiger, On the Reynolds stresses in mean-field hydrodynamics III. Two-dimensional turbulence and the problem of differential rotation, *Astron. Nachr.* **295**, 229-252 (1974)
- G. Rüdiger, L. L. Kitchatinov, A. Brandenburg, Cross helicity and turbulent magnetic diffusivity in the solar convection zone, *Solar Phys.* **269**, 3-12 (2011)
- R. Santos-Lima, A. Lazarian, E.M. de Gouveia Dal Pino, J. Cho, Diffusion of magnetic field and removal of magnetic flux from clouds via turbulent reconnection, *Astrophys. J.* **714**, 442-461 (2010)
- R. Santos-Lima, E.M. de Gouveia Dal Pino, A. Lazarian, The role of turbulent magnetic reconnection in the formation of rotationally supported protostellar disks, *Astrophys. J.* **747**, 21 (2012)
- A.A. Schekochihin, J.L. Maron, S.C. Cowley, J.C. McWilliams, The small-scale structure of magnetohydrodynamic turbulence with large magnetic Prandtl numbers, *Astrophys. J.* **576**, 806-813 (2002)
- A.A. Schekochihin, S.C. Cowley, J.L. Maron, J.C. McWilliams, Critical magnetic Prandtl number for small-scale dynamo, *Phys. Rev. Lett.* **92**, 054502 (2004a)
- A.A. Schekochihin, S.C. Cowley, S.F. Taylor, J.L. Maron, J.C. McWilliams, Simulations of the small scale turbulent dynamo, *Astrophys. J.* **612**, 276-307 (2004b)
- A.A. Schekochihin, N.E.L. Haugen, A. Brandenburg, S.C. Cowley, J.L. Maron, J.C. McWilliams, Onset of small scale dynamo at small magnetic Prandtl numbers, *Astrophys. J.* **625**, L115-L118 (2005)
- R. Schlickeiser, *Cosmic Ray Astrophysics*. Astron. Astrophys. Lib. Berlin: Springer (2002)
- J.V. Shebalin, W.H. Matthaeus, D. Montgomery, Anisotropy in MHD turbulence due to a mean magnetic field, *J. Plasm. Phys.* **29**, 525-547 (1983)
- A. Skumanich, Time scales for CA II emission decay, rotational braking, and lithium Depletion, *Astrophys. J.* **171**, 565-567 (1972)
- C.W. Smith, J.W. Bieber, Detection of steady magnetic helicity in low-frequency IMF turbulence, In 23rd International Cosmic Ray Conference, Vol. 3 (ed. D. A. Leahy, R. B. Hicks, and D. Venkatesan), pp. 493-496. Singapore: World Scientific (1993)
- S. Spangler, C. Gwinn, Evidence for an inner scale to the density turbulence in the interstellar medium, *Astrophys. J.* **353**, L29-L32 (1990)
- S. Stanimirovic, L. Staveley-Smith, J.M. Dickey, R.J. Sault, S.L. Snowden, The large-scale HI structure of the Small Magellanic Cloud, *Monthly Notices Roy. Astron. Soc.* **302**, 417-436 (1999)
- L.G. Stenholm, Molecular cloud fluctuations. II - Methods of analysis of cloud maps, *Astron. Astrophys.* **232**, 495-509 (1990)
- K. Subramanian, Can the turbulent galactic dynamo generate large-scale magnetic fields? *Monthly Notices Roy. Astron. Soc.* **294**, 718-728 (1998)
- S. Sur, A. Brandenburg, and K. Subramanian, Kinematic alpha effect in isotropic turbulence simulations, *Monthly Notices Roy. Astron. Soc.* **385**, L15-L19 (2008)
- H. Tennekes, J.L. Lumley, *First course in turbulence*. Cambridge: MIT Press (1972)
- A.G. Tevzadze, L. Kisslinger, A. Brandenburg, T. Kahniashvili, Magnetic Fields from QCD Phase Transitions, *Astrophys. J.* **759**, 54 (2012)
- H. Yan, A. Lazarian, Scattering of cosmic rays by magnetohydrodynamic turbulence, *Phys. Rev. Lett.* **89**, 281102 (2002)
- H. Yan, A. Lazarian, Cosmic-ray scattering and streaming in compressible magnetohydrodynamic turbulence, *Astrophys. J.* **614**, 757-769 (2004)
- H. Yan, A. Lazarian, Cosmic-ray propagation: nonlinear diffusion parallel and perpendicular to mean magnetic field, *Astrophys. J.* **673**, 942-953 (2008)
- S.I. Vainshtein, Ya.B. Zeldovich, Origin of magnetic fields in astrophysics, *Sov. Phys. Usp.* **15**, 159-172 (1972)
- J. Warnecke, P.J. Käpylä, M.J. Mantere, A. Brandenburg, Solar-like differential rotation in a convective dynamo with a coronal envelope, *Astrophys. J.*, submitted, arXiv:1301.2248 (2013)